Damping control of polodes, inertia and natural frequencies: theory and application to automotive suspensions

Simone Mesbahi [a], Silvia Milana [a], Antonio Culla [a], Gianluca Pepe [a],

Nicola Roveri [a], Antonio Carcaterra [a,*]

[a] *Department of Mechanical and Aerospace Engineering, La Sapienza University, Via Eudossiana 18, 00184 Rome, Italy*

[*] Corresponding author.
E-mail address: antonio.carcaterra@uniroma1.it (A. Carcaterra)

Acknowledgements

This work is supported by University of Rome, La Sapienza.

Declaration of interests

☒ The authors declare that they have no known competing financial interests or personal relationships that could have appeared to influence the work reported in this paper.

☐The authors declare the following financial interests/personal relationships which may be considered as potential competing interests:

[*] Corresponding author.
E-mail address: antonio.carcaterra@uniroma1.it (A. Carcaterra)

Abstract

This paper shows how tunable dampers can help control the instant centre of rotation of a 2D rigid body and its polode in planar motion, which in turn implies that the inertia tensor can also be controlled. For mechanisms equipped with some elasticity the results show that damping can also control their natural frequencies. The foundation of a general theory to control the polode is presented, exploring the chance of an optimal control formulation of the problem via a variational control principle, approached by the LQR (Linear Quadratic Regulator) method, after a suitable linearization. Application to automotive suspension linkages is presented that demonstrates the control of the instant roll centre and axis and consequently its instant roll vibration frequency to optimize the response, when excited by lateral inertia forces.

Keywords: semi-active damping, control, vibrations, polodes, instant centre, automotive

Introduction

Mechatronics in modern engineering is a powerful technology that enables achieving performances that purely mechanical devices cannot obtain. The field of automotive engineering is one of the branches that employs this technology at any level. Interestingly, mechatronics helps in making revolutions in traditional mechanical devices with ancient origin and for which the use of electronics, optics, electro-mechanical and control engineering produces an extraordinary injection of novelty [1,2]. It is clear, for example, how the mechatronic technology is progressively permeating both suspension and tire technologies, improving fundamental but old mechanical components [3-5]. For example, suspension devices in many cases employ tunable dampers that control internal dissipation effects by active and semi-active control technology, evidencing an increasing technical and scientific interest in this area.

Nowadays, damping represents the main object of semi-active controllers, since can be easily controlled through sophisticated damping devices, which permit to change the damping coefficient of the viscous fluid by modifying its rheological properties through voltage control [6-14]. Depending on the working principle, such smart actuators are classified as Magneto-Rheological (MR) dampers, if the change in fluid characteristics is based on the variation of the magnetic field within the damper, and Electro-Rheological (ER) ones, if the rheology depends on the applied electric field. Since they guarantee very fast responses and a large range for the eligible dissipative force, their usage has become a standard in semi-active control applications.

In general, the semi-active control of the impedance parameters of a system, i.e. stiffness and damping, by tunable actuators has been largely explored in many different fields such as in civil engineering for seismic protection of buildings [15], in robotics for trajectory-tracking problems [16,17], in acoustics to reduce the elastic vibrations and acoustic noise [18]. Nevertheless, its fundamental expression falls in the vehicle context [19-30] by equipping the suspension architectures with tunable-stiffness and/or tunable-damping actuators to improve the vehicle performances and mitigate its oscillatory motion depending on the working scenarios.

This paper belongs to the semi-active control field, but it is devoted to show how dampers can be used for both the kinematic guidance of a rigid mechanism, for path and motion generation purposes and to indirectly modify the inertial properties of a rigid body system, by modifying its polodes and, in turn, its natural frequencies.

This investigation differs from previous works. Jensen [31] proposed a polode synthesis method where the concepts of centrodes and polodes are used to synthesize planar mechanisms for path generation and motion generation purposes. Fu *et al.* [32] established a synthesis procedure to construct a spherical four-bar linkage by analysing the polodes and their derivatives, in a way that the motion of the coupler matches a given spherical motion up to a certain order. Jimenez *et al.* [33] proposed a general method for the optimum kinematic synthesis of multibody systems, where the design parameters are provided as output of a minimization problem of an objective function with respect to some geometric and functional constraints. Russel *et al.* [34] presented an instant screw axis approach for the precision point synthesis of a RRSS motion generator, by specifying a set of successive points to the instantaneous screw axis. Bai *et al.* [35] described a synthesis method for constructing minimally invasive robot mechanisms characterized by two or multiple remote centres of motion. Wang *et al.* [36] defined a new approach for the rigid body guidance where the adaptive curve fitting method is applied for the optimum synthesis of spherical four-bar linkages. Finally, Cera *et al.* [37] developed a path-constrained points synthesis method for the kinematic synthesis of higher-order path generator mechanisms, by prescribing higher-order curvature features.

While these studies are focused on investigating different ways to synthesize mechanisms for kinematic guidance tasks, the present research, in a similar fashion, offers a method to kinematically emulate reference mechanisms by changing the kinematics of the constraints through a suitable tuning of the corresponding damping coefficients. Moreover, the aim is to describe a general theory that shows how damping can affect the inertia parameters of a mechanical system. In fact, we show how the kinematic and inertial characteristics of a rigid body depend on the viscosity coefficients of the dampers included in a system of restraining linkages and, consequently, how the dampers control its instantaneous natural frequencies.

The use of dissipation to control the inertia properties of a body is new and is of practical interest. In fact, technically, the inertia tensor is difficult to be directly controlled by variable masses in a rigid body system, while its indirect control can be achieved through the usage of semi-active dampers that can be tuned in real-time simply by modulating electrical currents within the actuators.

This idea is illustrated in a simple form in section 2, starting from an elemental example in which the different settings of two tunable dampers can modify the instant centre of rotation of the body and, as a consequence, its natural frequency. Moreover, by taking advantage of the Hamilton's variational principle together with the Lagrangian multipliers method [38], the proposed approach unveils a general relationship between the dampers tuning and the inertia effects.

In section 3, the control of the instant centre of a moving body in planar motion is investigated, suggesting how its moment of inertia can be strongly influenced by the action of the dampers.

Once the equations of motion of the system are determined, and the equivalent damping is found, the problem of optimal control is attacked in the context of OCT (Optimal Control Theory) [39-44]. Through a suitable linearization of the problem, the LQR control method is applied, and the results are very encouraging.

Finally, in section 4, the technique illustrated in sections 2 and 3 is applied to the control of the motion of a more complex system, the suspensions of a car. In this case, it is shown how the combined effect of the kinematic control of the car body through the dampers modifies its roll moment of inertia and, as an effect, its oscillation frequencies, with benefits in the roll response under harmonic excitation. In fact, a particular linkages arrangement, defined as multi-damper suspension system, is employed to progressively modify the suspension kinematics and its instant roll centre position and, finally, the instant roll frequency of the car. Suitably implemented, the present control method permits the car body to better react to the lateral inertia forces, invariably born when the car is turning, especially along sequential wild left-right steering maneuvers.

2. Control of inertial properties and natural frequencies of the body by tunable dampers

The general idea presented here is varying the inertial characteristics of a body through the semi-active control [15-30] of its inertia tensor, based on the real-time variation of the damping coefficients [6-14] that characterize the constraints of the system. As a consequence, the natural frequencies of the system change too.

2.1. Fixed polode and equivalent inertia tensor of a rigid body

The position $\boldsymbol{x}_{IC}$ of the instant centre of rotation IC of a rigid body simply is:

$$\boldsymbol{x}_{IC} = \boldsymbol{x}_G + \frac{\boldsymbol{\omega}\ x\ \boldsymbol{v}_G}{|\boldsymbol{\omega}|^2} \tag{1}$$

where $\boldsymbol{\omega}$ is the angular velocity vector of the body. The parametric curve $\boldsymbol{x}_{IC}(t)$ when varying t is the fixed polode [38].

To show the change of the inertial characteristics of the body, the *equivalent inertia tensor* $\boldsymbol{J}_{eq}$ is computed, the components of which are in the frame with origin IC, and axes oriented as the fixed reference frame.

The Huygens-Steiner theorem states:

$$\boldsymbol{J}_{eq} = \boldsymbol{R}\boldsymbol{J}'_G\boldsymbol{R}^T + \boldsymbol{J}_{HS} \tag{2}$$

where $\boldsymbol{J}'_G$ is the inertia tensor of the body with respect to its mobile reference frame centred in G, $\boldsymbol{R}$ is the rotation matrix between mobile and fixed reference frames, $\boldsymbol{J}_{HS} = m|\boldsymbol{x}_{IC} - \boldsymbol{x}_G|^2$, *i.e.* it depends on the body mass and the squared distance between G and IC. Therefore, the proposed method indirectly controls $\boldsymbol{J}_{eq}$, by controlling the fixed polode of the body.

Finally, the change and control of the natural frequencies is a consequence of controlling $\boldsymbol{J}_{eq}$.

2.2. An elemental example

To show in the simplest way the concept investigated here, consider a planar mechanism restraining a square rigid body B of dimension 2*l*, as represented in Fig. 1, characterized by the presence of two springs, with stiffness k, a rigid link, and a pair of telescopic links, both equipped with tunable dampers, whose characteristic damping coefficients are c_1 and c_2.

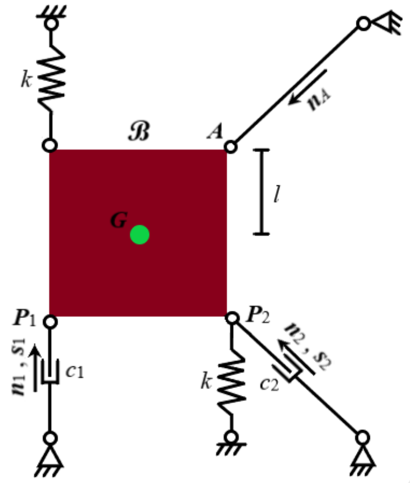

Fig. 1. Planar mechanism.

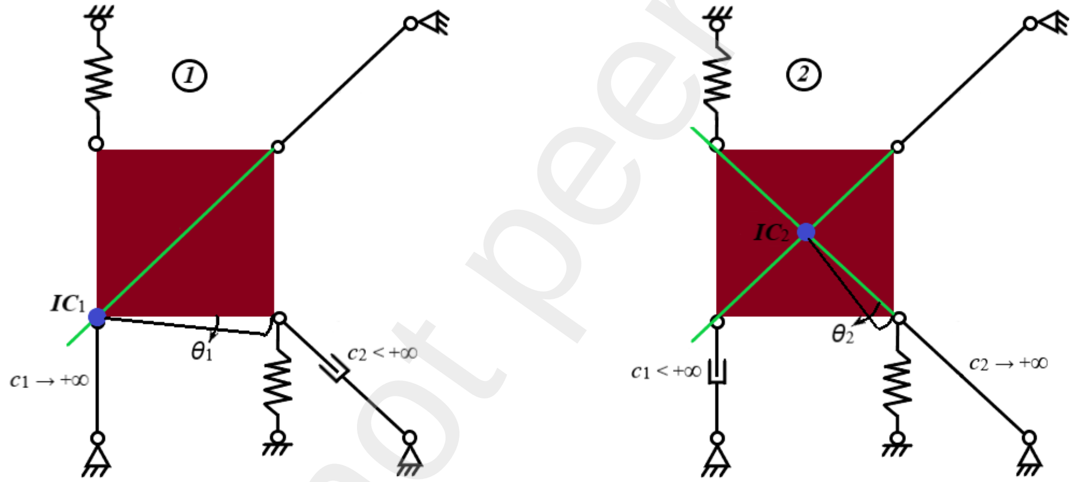

Fig. 2. Migration of the instant centre of rotation due to change in damping coefficients settings.

A simple kinematic analysis shows 2 d.o.f. for a general regulation of the parameters c_1 and c_2. If s_1 and s_2 represent the axial displacements along the directions $\boldsymbol{n}_1$ and $\boldsymbol{n}_2$ of the links axes, the corresponding intensity of the axial forces can be modelled simply as $c_1\dot{s}_1$ and $c_2\dot{s}_2$, respectively, assuming viscous velocity-proportional actions (note that more complicated constitutive relationships can be adopted, without significant modifications of the proposed approach).

One could set, for example, c_1 very large (leaving c_2 small enough) so that the corresponding sliding guide becomes axially rigid. An analogous condition is obtained for c_2 large and c_1 small. In both cases (1: $c_1 \rightarrow +\infty$, $c_2 < +\infty$ or 2: $c_1 < +\infty$, $c_2 \rightarrow +\infty$) the 2 d.o.f. system collapses into a single d.o.f. mechanism. This leads to a change of the overall kinematics of the body, and remarkably to the change of the position of its instant centre of rotation IC, as it can be observed in Fig. 2.

This simple example demonstrates how the settings of both c_1 and c_2 can affect the inertial characteristics of the body causing the migration of its instant centre position from IC_1 to IC_2, consequently making its inertia moment dependent on the two damping coefficients. How viscosity can affect the body inertia and how this effect is useful for the rigid body motion control is the main novelty investigated in this paper compared with the existing literature [15-30,31-37]. This inertia modification produces a change in the body natural frequencies as illustrated below.

In fact, if the damping coefficients of the linkages are set as in case 1, the instant centre of rotation collapses to IC_1 and, in this configuration, the body shows a single d.o.f. represented by the rotation θ_1 about that point (see Fig. 2). In this circumstance, the Lagrangian function of the system is:

$$L = \frac{1}{2}J_b^1\dot{\theta}_1^{\,2} - \frac{1}{2}k(2l\theta_1)^2 \tag{3}$$

with $J_b^1 = J_G + 2ml^2$ the *equivalent moment of inertia* of the body with respect to IC_1, where $J_G = \frac{2}{3}ml^2$ is the moment of inertia of the body with respect to G and m the body mass.

From Eq. (3) it is easy to derive the equation of motion of the system:

$$J_b^1\ddot{\theta}_1 + 4kl^2\theta_1 = 0 \tag{4}$$

and its natural frequency:

$$\omega_n^{(1)} = \sqrt{\frac{4l^2k}{J_b^1}} = \sqrt{\frac{4l^2k}{J_G + 2ml^2}} = \sqrt{\frac{3k}{2m}} \tag{5}$$

If the damping coefficients are set as in case 2, the instant centre of rotation migrates to IC_2 (which in this case coincides with G, *i.e.* the centre of the square) and, in this configuration, the only available d.o.f. is described by the rotation θ_2 about this point (see Fig. 2).

Therefore, the system now behaves according to the new dynamic equation:

$$J_{sq}\ddot{\theta}_2 + 2kl^2\theta_2 = 0 \tag{6}$$

with natural frequency:

$$\omega_n^{(2)} = \sqrt{\frac{2l^2k}{J_G}} = \sqrt{\frac{3k}{m}} \tag{7}$$

Thus, the comparison between the two determined natural frequencies in Eq. (5) and Eq. (7) shows clearly how the setting of the dampers can affect the resonance response of the analysed system.

This effect can be investigated in general for arbitrarily complex systems in the next section.

2.3. General method

The general method relies on the use of a set of Lagrangian variables that include 6 components for the rigid body motion in 3D (only 3 components in 2D), and a number *N* of axial sliding variables s_j (j = 1, …, N), associated to an equal number of telescopic linkages. For example, the Lagrangian variables in Fig. 3 are chosen as $x_G, y_G, z_G, \varphi, \theta, \psi, s_1, ..., s_N$, the first three are associated with the gravity centre position G, the second set of three with the body rotation and the last *N* are the auxiliary variables introduced to represent the axial displacements of the links. Since the total number of variables is higher than the 6 strictly necessary variables to describe the rigid body motion, constraints among the selected variables must be introduced:

$$\boldsymbol{v}_{P_j} \cdot \boldsymbol{n}_j - \dot{s}_j = 0 \quad j = 1,...,N \tag{8}$$

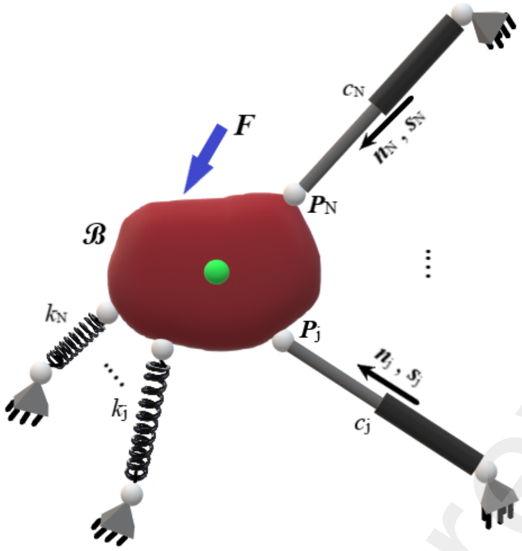

Fig. 3. General 3D rigid body constrained with telescopic links and springs.

where $\boldsymbol{n}_j$ is the axial direction of the j-th telescopic linkage and $\boldsymbol{v}_{P_j}$ is the velocity of the point P_j (see Fig. 3) provided by the fundamental formula of kinematics as:

$$\boldsymbol{v}_{P_j} = \boldsymbol{v}_G + \boldsymbol{\Omega}\boldsymbol{x}_{GP_j} \tag{9}$$

with $\boldsymbol{\Omega}$ the skew-symmetric matrix of the body angular velocities and $\boldsymbol{x}_{GP_j}$ the vector from G to P_j.

In the case of Fig. 1, the mechanism is two-dimensional, so the Lagrangian variables are x_G, y_G, φ, s_1, s_2. These 5 variables are constrained by 3 equations, and $\boldsymbol{v}_{P_1}$ and $\boldsymbol{v}_{P_2}$ depend on x_G, y_G, φ and their derivatives through the fundamental formula of kinematics in Eq. (7). More precisely, the constraint equations are:

$$\begin{cases} \boldsymbol{v}_{P_1} \cdot \boldsymbol{n}_1 - \dot{s}_1 = 0 \\ \boldsymbol{v}_{P_2} \cdot \boldsymbol{n}_2 - \dot{s}_2 = 0 \\ \boldsymbol{v}_A \cdot \boldsymbol{n}_A = 0 \end{cases} \tag{10}$$

where the last equation imposes that the velocity of the point of the body connected with the rigid linkage is orthogonal to its longitudinal axis. In the general case of 3D, the set of constraint equations between the total set of Lagrangian variables x_G, y_G, z_G, φ, θ, ψ, s_1, ..., s_N can be written in the form:

$$a_j(\boldsymbol{q},\dot{\boldsymbol{q}}) - \dot{s}_j = 0 \quad j = 1,\ldots,N \tag{11}$$

where $a_j(\boldsymbol{q},\dot{\boldsymbol{q}}) = \boldsymbol{v}_{P_j} \cdot \boldsymbol{n}_j$ with $\boldsymbol{q},\dot{\boldsymbol{q}}$ the vectors of the Lagrangian variables and their derivatives associated with the 6 body d.o.f. In particular, $\boldsymbol{q}$ can be partitioned as follows:

$$\boldsymbol{q} = \begin{bmatrix} \boldsymbol{q}^{(G)} \\ - \\ \boldsymbol{q}^{(R)} \end{bmatrix} = \begin{bmatrix} x_G \\ y_G \\ z_G \\ - \\ \varphi \\ \theta \\ \psi \end{bmatrix} \tag{12}$$

to separate the translational d.o.f. from the rotational ones.

Considering the presence of possible external forces acting on the body and also elastic potential forces, an elegant way to approach the system dynamics is the application of the Hamilton's variational principle together with the Lagrangian multipliers method [38].

The Hamiltonian functional is defined through an integral over a generic observation time $\overline{T}$, as:

$$H = \int_0^{\overline{T}} \{K(\boldsymbol{q},\dot{\boldsymbol{q}}) - U(\boldsymbol{q}) + \sum_{j=1}^{N} \lambda_j [a_j(\boldsymbol{q},\dot{\boldsymbol{q}}) - \dot{s}_j]\}\, dt \tag{13}$$

where H depends on the kinetic energy of the system K, on its potential energy U and on the constraint relationships in Eq. (11) through the introduction of the Lagrangian multipliers λ_j. Moreover, the virtual work of the non-conservative external forces is:

$$\delta W_n = \sum_{i=1}^{6} Q_i \delta q_i - \sum_{j=1}^{N} c_j \dot{s}_j \delta s_j \tag{14}$$

where Q_i are the Lagrangian components of the external forces acting on the virtual displacements δq_i and c_j $\dot{s}_j$ the virtual works done by the viscous forces on the virtual displacements δs_j.

The Hamilton's principle states:

$$\delta H + \int_0^{\overline{T}} \delta W_n \, dt = 0 \tag{15}$$

$$\delta \int_0^{\overline{T}} \{K(\boldsymbol{q},\dot{\boldsymbol{q}}) - U(\boldsymbol{q}) + \sum_{j=1}^{N} \lambda_j [a_j(\boldsymbol{q},\dot{\boldsymbol{q}}) - \dot{s}_j]\} dt + \int_0^{\overline{T}} \delta W_n \, dt = 0 \tag{16}$$

$$\int_0^{\overline{T}} \left\{ \sum_{i=1}^{6} \left[\left(\frac{\partial K}{\partial q_i} - \frac{\partial U}{\partial q_i} \right) \delta q_i + \frac{\partial K}{\partial \dot{q}_i} \delta \dot{q}_i \right] + \sum_{j=1}^{N} \delta\lambda_j [a_j - \dot{s}_j] + \sum_{j=1}^{N} \lambda_j \left[\sum_{i=1}^{6} \left(\frac{\partial a_j}{\partial q_i} \delta q_i + \frac{\partial a_j}{\partial \dot{q}_i} \delta \dot{q}_i \right) \right] - \sum_{j=1}^{N} \lambda_j \delta \dot{s}_j + \sum_{i=1}^{6} Q_i \delta q_i - \sum \right. \tag{17}$$

Taking advantage of the integration by parts, neglecting the boundary conditions, grouping the terms associated respectively with the 3 independent perturbations δq_i, δs_j, $\delta \lambda_j$, the following three sets of equations hold:

$$\frac{\partial K}{\partial q_i} - \frac{\partial U}{\partial q_i} - \frac{d}{dt}\frac{\partial K}{\partial \dot{q}_i} + \sum_{j=1}^{N} \lambda_j \frac{\partial a_j}{\partial q_i} - \sum_{j=1}^{N} \dot{\lambda}_j \frac{\partial a_j}{\partial \dot{q}_i} - \sum_{j=1}^{N} \lambda_j \left[\sum_{r=1}^{N} \left(\frac{\partial^2 a_j}{\partial \dot{q}_i \partial q_r} \dot{q}_r + \frac{\partial^2 a_j}{\partial \dot{q}_i \partial \dot{q}_r} \ddot{q}_r \right) \right] + Q_i = 0 \quad i = 1,\ldots,6 \tag{18}$$

$$\dot{\lambda}_j - c_j \dot{s}_j = 0 \quad j = 1,\ldots,N \tag{19}$$

$$a_j(\boldsymbol{q},\dot{\boldsymbol{q}}) - \dot{s}_j = 0 \quad j = 1,\ldots,N \tag{20}$$

By considering both Eq. (19) and Eq. (20), a simple relationship between λ_j and c_j emerges:

$$\dot{\lambda}_j = c_j \dot{s}_j = c_j a_j \tag{21}$$

The coefficients c_j are functions of time, as well as the a_j's, since they depend on the Lagrangian variables. Eq. (18)-(21) shows the way the control vector $\boldsymbol{c} = [c_j]$ appears in the equation of motion. Our goal is to control the motion of the body through $\boldsymbol{c}$. The form of these equations show the problem is highly nonlinear, and difficult to solve in general. For this reason, it is solved recurring to a time-by-time linearization to apply an algorithm of control that is robust, the Linear Quadratic Regulator (LQR) [45]. This approach is used in the next sections.

A first question emerges: how do the coefficients c_j affect the inertial properties of the body, *i.e.*, how do the controllable terms c_j appear into the inertial terms?

The only terms in Eq. (18) associated with the inertial properties of the system are those containing $\ddot{\boldsymbol{q}}$, *i.e.*:

$$-\frac{d}{dt}\frac{\partial K}{\partial \dot{q}_i}(\boldsymbol{q},\dot{\boldsymbol{q}}) - \sum_{j=1}^{N} \lambda_j \left[\sum_{r=1}^{6} \left(\frac{\partial^2 a_j}{\partial \dot{q}_i \partial \dot{q}_r} \ddot{q}_r\right)\right] \quad (22)$$

that, in fact, is:

$$\sum_{r=1}^{6} \left(\frac{\partial^2 K}{\partial \dot{q}_i \partial q_r} \dot{q}_r + \frac{\partial^2 K}{\partial \dot{q}_i \partial \dot{q}_r} \ddot{q}_r\right) - \sum_{j=1}^{N} \lambda_j \left[\sum_{r=1}^{6} \left(\frac{\partial^2 a_j}{\partial \dot{q}_i \partial \dot{q}_r} \ddot{q}_r\right)\right] \quad (23)$$

However, since the terms a_j are linear in the Lagrangian velocity components, it can be demonstrated that:

$$\frac{\partial^2 a_j}{\partial \dot{q}_i \partial \dot{q}_r} = 0 \quad (24)$$

Therefore, the inertial effects remain with the terms $\sum_{r=1}^{6} \left(\frac{\partial^2 K}{\partial \dot{q}_i \partial \dot{q}_r} \ddot{q}_r\right)$.

Now, by considering the expression for the velocity of the point P_j in Eq. (9):

$$\boldsymbol{\Omega} = \dot{\boldsymbol{R}}(\boldsymbol{q}^{(R)},\dot{\boldsymbol{q}}^{(R)})\boldsymbol{R}^T(\boldsymbol{q}^{(R)}) \quad (25)$$

$$\boldsymbol{v}_G = \dot{\boldsymbol{q}}^{(G)} \quad (26)$$

and:

$$\boldsymbol{v}_{P_j} = \dot{\boldsymbol{q}}^{(G)} + \boldsymbol{M}_j(\boldsymbol{q})\dot{\boldsymbol{q}}^{(R)} \quad (27)$$

with:

$$\boldsymbol{M}_j(\boldsymbol{q})\dot{\boldsymbol{q}}^{(R)} = \dot{\boldsymbol{R}}(\boldsymbol{q}^{(R)},\dot{\boldsymbol{q}}^{(R)})\boldsymbol{R}^T(\boldsymbol{q}^{(R)})\boldsymbol{x}_{GP_j} \quad (28)$$

By substituting the expression in Eq. (27) into Eq. (11), it holds:

$$\dot{\boldsymbol{q}}^{(G)} \cdot \boldsymbol{n}_j(\boldsymbol{q}) + \boldsymbol{M}_j(\boldsymbol{q})\dot{\boldsymbol{q}}^{(R)} \cdot \boldsymbol{n}_j(\boldsymbol{q}) = \dot{s}_j \quad (29)$$

$$\dot{\boldsymbol{q}}^{(G)} \cdot \boldsymbol{n}_j(\boldsymbol{q}) + \boldsymbol{M}_j^T(\boldsymbol{q})\boldsymbol{n}_j(\boldsymbol{q}) \cdot \dot{\boldsymbol{q}}^{(R)} = \dot{s}_j \quad (30)$$

that written in a more compact form is:

$$\left[\boldsymbol{n}_j^T(\boldsymbol{q}) \quad \boldsymbol{n}_j^T(\boldsymbol{q})\boldsymbol{M}_j(\boldsymbol{q})\right]\dot{\boldsymbol{q}} = \boldsymbol{w}_j^T(\boldsymbol{q})\dot{\boldsymbol{q}} = \dot{s}_j \quad j = 1,\ldots,N \quad (31)$$

Derivation of Eq. (31) with respect to time yields:

$$\left[\frac{\partial \boldsymbol{w}_j^T}{\partial \boldsymbol{q}}\dot{\boldsymbol{q}}\right]\dot{\boldsymbol{q}} + \boldsymbol{w}_j^T(\boldsymbol{q})\ddot{\boldsymbol{q}} = \ddot{s}_j \quad j = 1,\ldots,N \quad (32)$$

By deriving with respect to time the expression for $\dot{s}_j$ from Eq. (19) and then by substituting it into the previous equation, one obtains:

$$\boldsymbol{w}_j^T\ddot{\boldsymbol{q}} = \frac{1}{c_j}\left[\dot{\lambda}_j - \dot{s}_j\dot{c}_j\right] - \left[\frac{\partial \boldsymbol{w}_j^T}{\partial \boldsymbol{q}}\dot{\boldsymbol{q}}\right]\dot{\boldsymbol{q}} \quad j = 1,\ldots,N \quad (33)$$

For example, in the particular case of $N = 6$, *i.e.* if the number of tunable dampers equals the number of degrees of freedom of the rigid body, Eq. (31) can provide the direct expression for $\dot{\boldsymbol{q}}$ in terms of the damping coefficients: $\dot{\boldsymbol{q}} = \boldsymbol{W}(\boldsymbol{q})\dot{\boldsymbol{s}}$, hence, by considering Eq. (21), $\dot{\boldsymbol{q}} = \boldsymbol{W}(\boldsymbol{q})\boldsymbol{C}^{-1}\dot{\boldsymbol{\lambda}}$ and $\ddot{\boldsymbol{q}} = \frac{\partial}{\partial \boldsymbol{q}}\boldsymbol{W}(\boldsymbol{q})\dot{\boldsymbol{q}}\,\boldsymbol{C}^{-1}\,\dot{\boldsymbol{\lambda}} + \boldsymbol{W}(\boldsymbol{q})\dot{\boldsymbol{C}}^{-1}\dot{\boldsymbol{\lambda}} + \boldsymbol{W}(\boldsymbol{q})\,\boldsymbol{C}^{-1}\,\ddot{\boldsymbol{\lambda}}$, with $\boldsymbol{C} = diag(c_j)$.

This implies that the inertial terms in the equation of motion, that are represented by $\sum_{r=1}^{6}\left(\frac{\partial^2 K}{\partial \dot{q}_i \partial \dot{q}_r}\ddot{q}_r\right)$, are affected by the tunable dampers through the control variables c_j. In fact, from Eq. (33), the implicit relationship between $\ddot{\boldsymbol{q}}$ and c_j emerges. As clarified by the simple examples in the introductory part of this section, the change of the inertial properties also affects the natural frequencies of the system.

After demonstrating that the inertia is affected by the setting of the dampers through the c_j, a second question is related to the control of $\boldsymbol{q}$ through the vector $\boldsymbol{c}$. The equations of motion are nonlinear since through Eq. (33) the control variables c_j are multiplied by the state auxiliary variables $\dot{s}_j$. Reduction of the previous problem to a linearized form is useful and proceeds as shown below in combination with the OCT technique [39-44].

2.4. An optimal control algorithm

OCT uses a key performance index (KPI) or *functional* J^*. It is defined through an integral over a prescribed observation time $\overline{T}$. J^* depends on the system response $\boldsymbol{x} = [\boldsymbol{q},\dot{\boldsymbol{q}}]^T$, on the adopted control $\boldsymbol{u}$ (that coincides with $\boldsymbol{c}$), and, in general, on the external uncontrolled force $\boldsymbol{y}$:

$$J^* = \int_0^{\overline{T}} \left\{|\boldsymbol{x} - \boldsymbol{x}_r|^2 + |\boldsymbol{u} - \boldsymbol{u}_r|^2\right\} dt \tag{34}$$

where $\boldsymbol{u}_r$ is the control required to guarantee that the state vector reaches the reference value $\boldsymbol{x}_r$. The statement of the control problem can be formulated as [39,40]:

$$min\ (\boldsymbol{x},\boldsymbol{u}) \quad J^* = \int_0^{\overline{T}} L(\boldsymbol{x},\boldsymbol{u},\boldsymbol{y}) dt \tag{35}$$

where L is called the *Lagrangian function* or *penalty function* and $\overline{U}$ is the admissible set of values for the control solution $\boldsymbol{u}$. Furthermore, $\boldsymbol{u} \in \overline{U}$ and J^* is subject to the differential dynamic system equations constraint:

$$\begin{cases} \dot{\boldsymbol{x}} - \boldsymbol{f}(\boldsymbol{x},\boldsymbol{u},\boldsymbol{y}) = \boldsymbol{0} \\ \boldsymbol{x}(0) = \boldsymbol{x}_0 \end{cases} \tag{36}$$

In case the system dynamics is linear, *i.e.* $\boldsymbol{f} = \boldsymbol{A}\boldsymbol{x} + \boldsymbol{B}\boldsymbol{u} + \boldsymbol{y}$, the LQR method can be applied [45], and the solution of the optimization problem leads to the subsequent control vector:

$$\boldsymbol{u} = \overline{\boldsymbol{R}}^{-1}\boldsymbol{B}^T[\boldsymbol{S}[\boldsymbol{x} - \boldsymbol{x}_r] + \boldsymbol{p}] + \boldsymbol{u}_r \tag{37}$$

where $\boldsymbol{S}$ and $\boldsymbol{p}$ are determined by the *Riccati's equation* and the *complementary equation,* respectively, as:

$$\begin{cases} \dot{\boldsymbol{S}} + \boldsymbol{A}^T\boldsymbol{S} + \boldsymbol{S}\boldsymbol{A} - \boldsymbol{S}\boldsymbol{B}\overline{\boldsymbol{R}}^{-1}\boldsymbol{B}^T\boldsymbol{S} + \overline{\boldsymbol{Q}} = \boldsymbol{0} \\ \dot{\boldsymbol{p}} + \boldsymbol{A}^T\boldsymbol{p} - \boldsymbol{S}\boldsymbol{B}\overline{\boldsymbol{R}}^{-1}\boldsymbol{B}^T\boldsymbol{p} + \boldsymbol{S}\boldsymbol{y} = \boldsymbol{0} \end{cases} \tag{38}$$

with boundary conditions:

$$\begin{cases} \boldsymbol{S}(\overline{T}) = \boldsymbol{0} \\ \boldsymbol{p}(\overline{T}) = \boldsymbol{0} \end{cases} \tag{39}$$

The linearization process can be systematically applied as the configuration of the system modifies when time is spent (see Appendix), and each sequential linearization is considered valid along the small-time interval during which the configuration does not modify sensibly. Along this time interval, since the differential problem is linear, natural frequencies can be considered as the eigenvalues associated with the given configuration about which the problem is linearized. Under this point of view, the inertia of the system and its instantaneous natural frequencies change through the control of the damping coefficients.

3. LQR control of the instant centre and the body inertia by four/eight sliding couplers

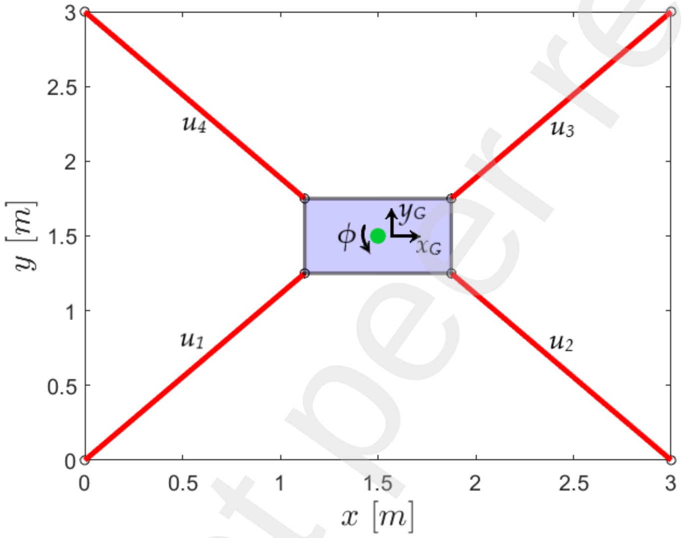

Fig. 4. 4-actuators mechanical system.

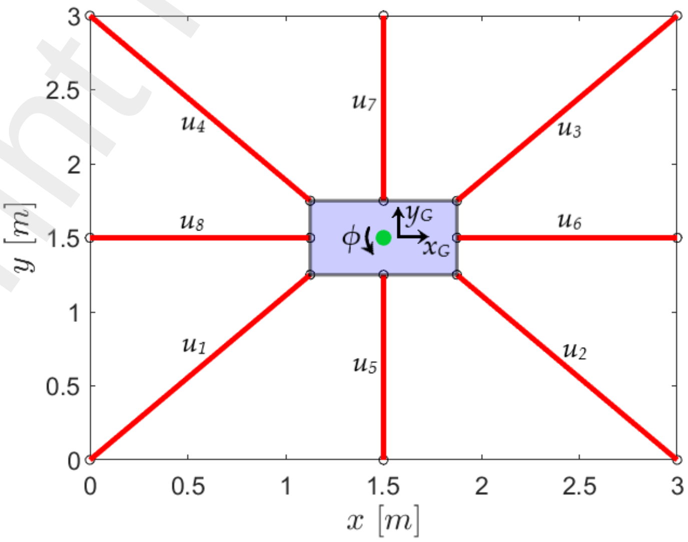

Fig. 5. 8-actuators mechanical system.

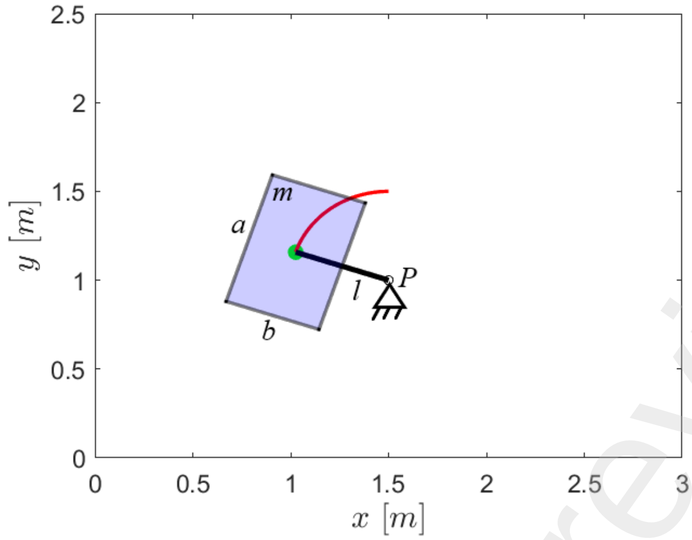

Fig. 6. Reference mechanism.

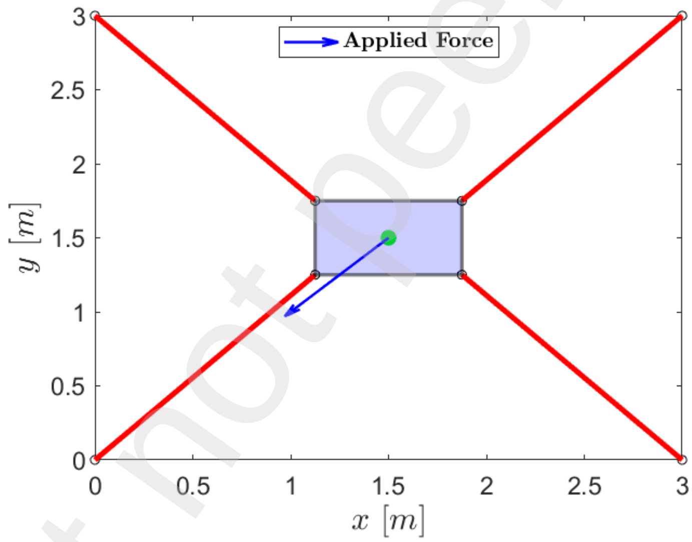

Fig. 7. External applied force.

The LQR algorithm is here applied to the control of the instant centre of rotation IC of a planar rigid body, *i.e.* of its fixed polode, and consequently of its inertia tensor.

The system model consists of a rigid rectangular body constrained through four or eight sliding linkages equipped with controllable dampers, as shown in Fig. 4 and 5, respectively.

Two cases are considered. The first, in Fig. 4, shows the 4-actuators system, while the second, in Fig. 5, the 8-actuators system, and the LQR method finds the optimal damping coefficients u_i to let the body kinematically emulate a reference mechanism, such as the pendulum system in Fig. 6.

It consists of a rigid body of mass $m = 1$ kg and dimensions $a = 0.75$ m, $b = 0.5$ m, which is hinged through a rigid pendulum of length $l = 0.5$ m to a point P. If the body is considered rigidly linked to the pendulum in its centre of gravity G, it undergoes a pure rotation around P.

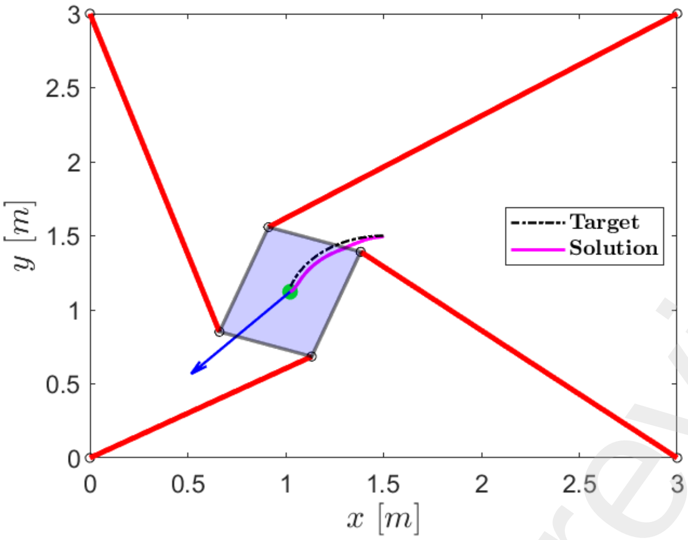

Fig. 8. Trajectory emulation of the 4-actuators system.

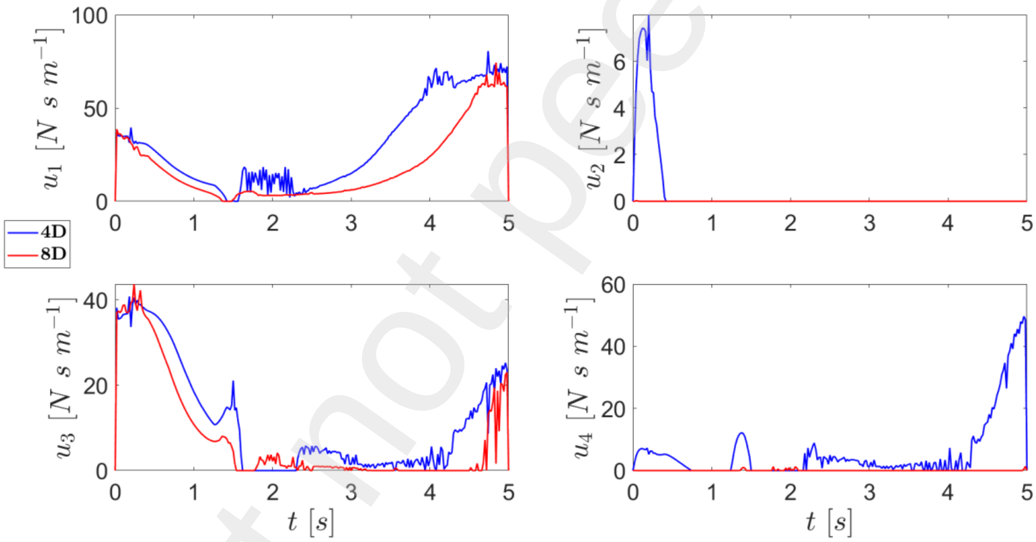

Fig. 9. Comparison between the optimal damping coefficients of the 4-actuators system (4D) and of the 8-actuators system (8D) for the same four actuators.

Therefore, the controller task is to guarantee that G remains over a circumference of given radius and centre P (see Fig. 6), that means the fixed polode of the body motion is imposed. In fact, in this particular scenario, the instant centre of rotation of the body must collapse exactly to point P.

The requirement on the instant centre of rotation determines an indirect modification of the inertial characteristics of the body, *i.e.*, of its moment of inertia with respect to the fixed frame.

Being x_G, y_G, ϕ the Lagrangian variables necessary to describe the rigid body motion (see Fig. 4 and 5), one could set the subsequent target state vector for the control problem, provided as laws of motion from the reference system:

$$\boldsymbol{x}_r = \begin{bmatrix} x_{G_r} & \dot{x}_{G_r} & y_{G_r} & \dot{y}_{G_r} & \phi_r & \dot{\phi}_r \end{bmatrix}^T \tag{40}$$

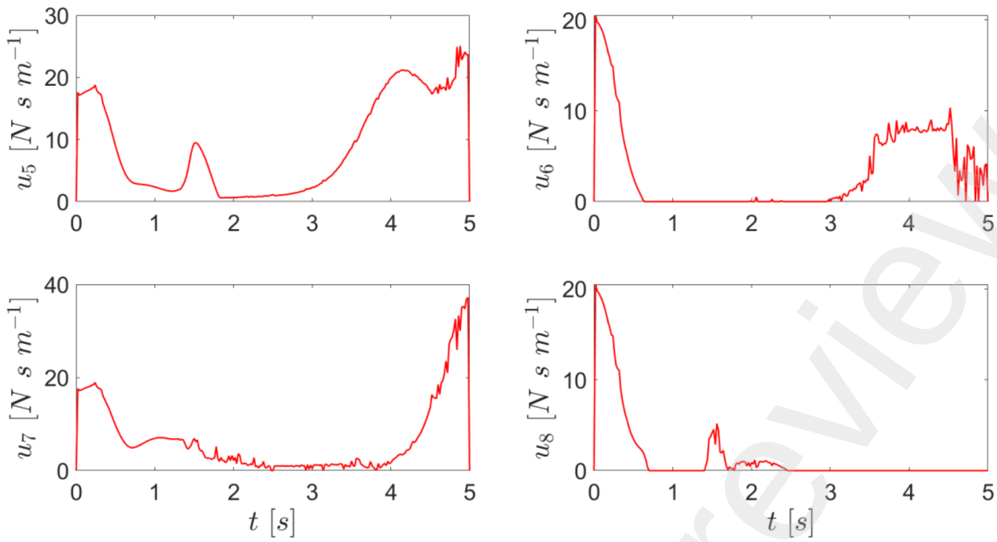

Fig. 10. Optimal damping coefficients of the four added actuators of the 8-actuators system.

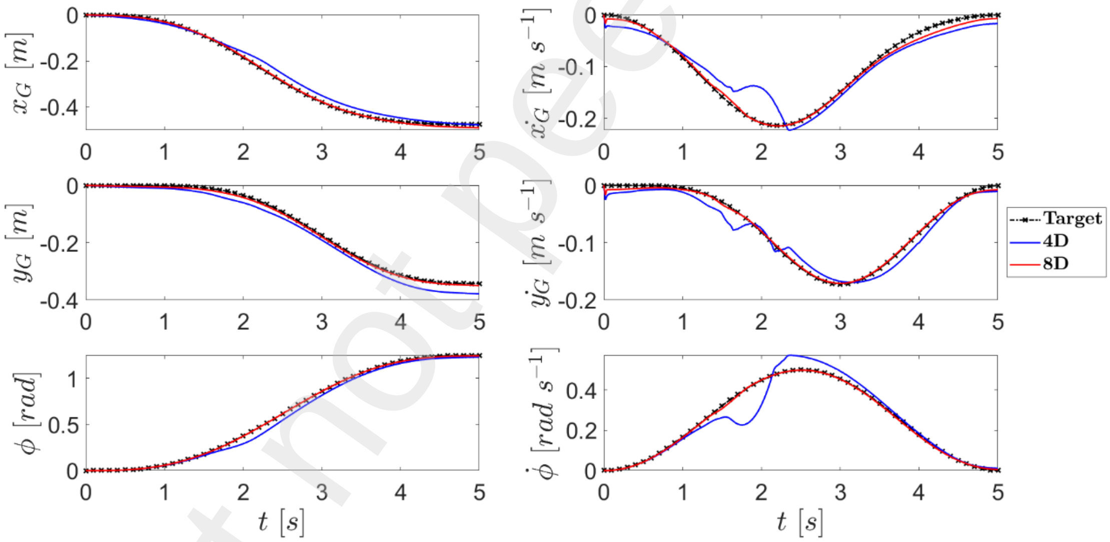

Fig. 11. Comparison between the solutions for the 4-actuators (4D) and 8-actuators (8D) systems and the target quantities provided by the reference mechanism.

where all the components are known functions of time, computed over an observation period $\overline{T} = 5$ s.

To induce a motion in the system, an external force is applied with constant magnitude at the centre of mass and directed towards the origin, as shown in Fig. 7 (any other choice is plausible, but without changing the strategy of the proposed method).

At each linearization step (see Appendix), the optimal damping vector $\boldsymbol{u}$ obtained by the LQR algorithm assumes the form:

$$\boldsymbol{u} = \overline{\boldsymbol{R}}^{-1}\boldsymbol{B}^T[\boldsymbol{S}[\boldsymbol{x} - \boldsymbol{x}_r] + \boldsymbol{p}] - \boldsymbol{\Theta}(\boldsymbol{x}_r)^+[\boldsymbol{\Phi}(\boldsymbol{x}_r) + \boldsymbol{y} - \dot{\boldsymbol{x}}_r] \tag{41}$$

The tracking of body rotation and its angular velocity poses a challenge for the control problem.

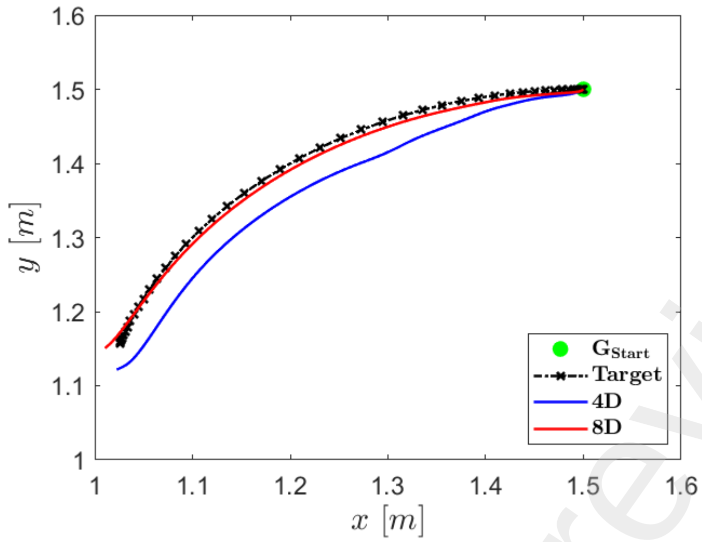

Fig. 12. Comparison between the trajectories of G for the 4-actuators (4D) and 8-actuators (8D) systems with the target trajectory provided by the reference mechanism.

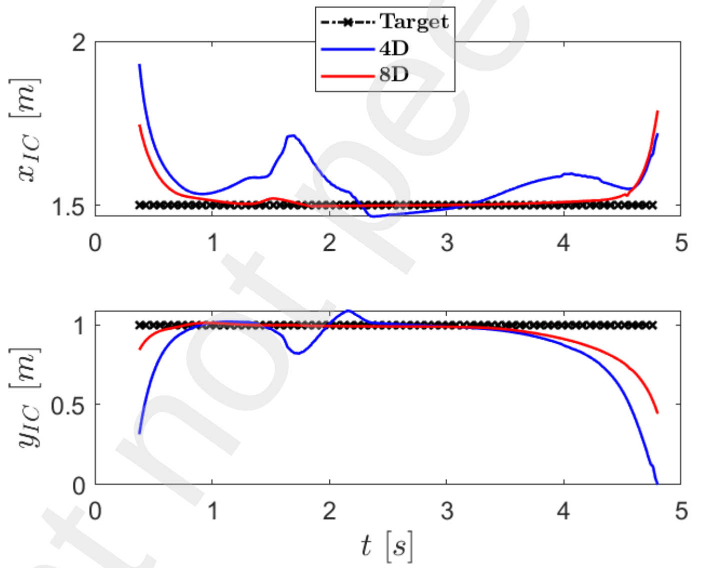

Fig. 13. Coordinates of the instant centre of rotation IC for the controlled solutions with respect to the corresponding targets provided by the reference mechanism.

Fig. 8 shows the controlled trajectory of G obtained by the control method described in Section 2 and in the Appendix for the 4-actuators system. The actual trajectory (violet solid line), as expected, does not exactly overlap with the desired target (black dashed line). One can expect that additional actuators can improve the quality of the solution. Indeed, in the next figures, the comparison between the 4-actuators system and the 8-actuators one is presented.

By observing the comparison of the optimal damping coefficients in Fig. 9, obtained through Eq. (41), one can notice how the 8-actuators system shows smoother solutions with reduced chattering, that indeed seems to characterize the case of the 4-actuators system.

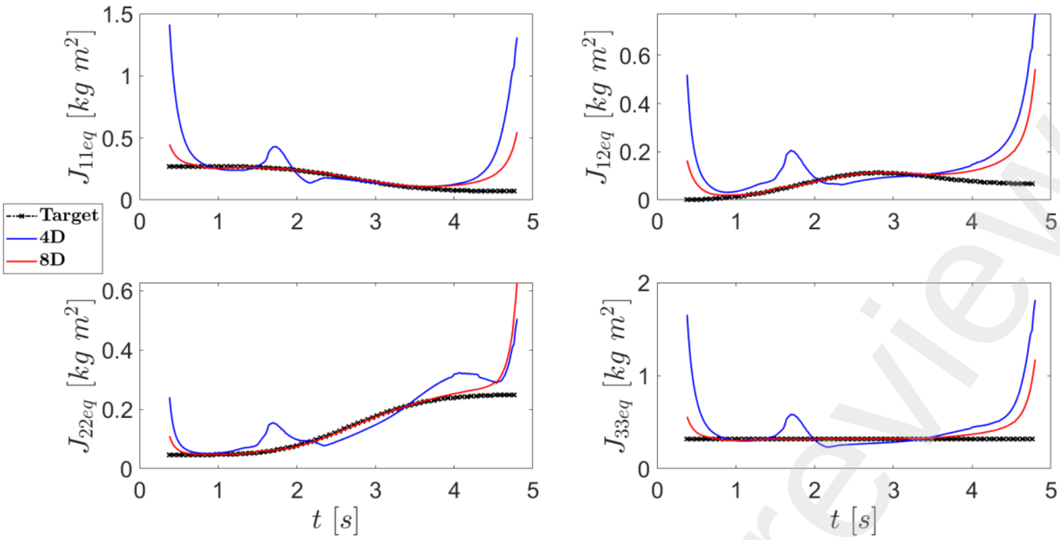

Fig. 14. Equivalent inertia tensor components of the controlled solutions with respect to the corresponding targets provided by the reference mechanism.

Fig. 11 and 12 shows the comparisons between the target quantities and the optimal solutions found by the controller. The 8-actuators configuration provides more accurate results by guaranteeing lower instabilities and better matching with the targets, with respect to the system equipped with 4 actuators only.

The coordinates of the corresponding IC, which define the fixed polode associated with these solutions and computed through Eq. (1), are shown in Fig. 13. These quantities are compared with the target values, which coincide with the coordinates of point P of the reference mechanism, *i.e.* the reference fixed polode (see Fig. 4).

The ability of the controller in tracking the polodes has its counterpart in controlling the inertial characteristics of the body. The better the polode tracking, the better the *equivalent inertia tensor* $\boldsymbol{J}_{eq}$ tracking, as it can be deduced by Fig. 14. This shows the non-zero components of the tensor, computed by Eq. (2), with $J_{21_{eq}} = J_{12_{eq}}$ and $J_{13_{eq}} = J_{23_{eq}} = J_{31_{eq}} = J_{32_{eq}} = 0$, since the body performs a planar motion.

Again, it is clear how the 8-actuators system is better in emulating the inertial properties of the reference system.

4. Automotive suspension system for instant roll centre control

The system illustrated in Fig. 15 is a double-arm suspension, which is a classic setup in automotive applications. The positions of the pivots of the linkages and their characteristic inclinations determine the position of the roll centre RC, which lies under the road plane. The instant centre position determines many important characteristics of the roll response of the car, together with some effects related to the interaction between yaw and roll motion (partly depending on the inclination of the roll axis with respect to the road plane).

An actively controlled suspension drives the position of the roll centre, depending on the operating conditions the car is approaching. This effect can be obtained by varying actively the positions of the pivots of the suspension system, but it is technically difficult, expensive, and not robust.

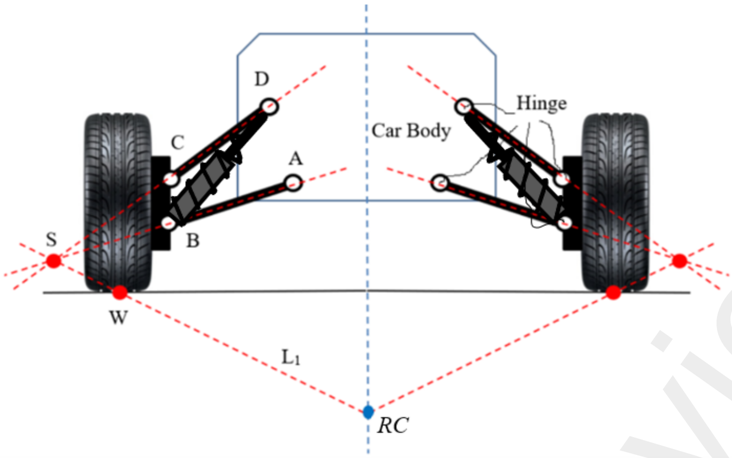

Fig.15. Classic double-arm suspension system with identification of the roll centre RC.

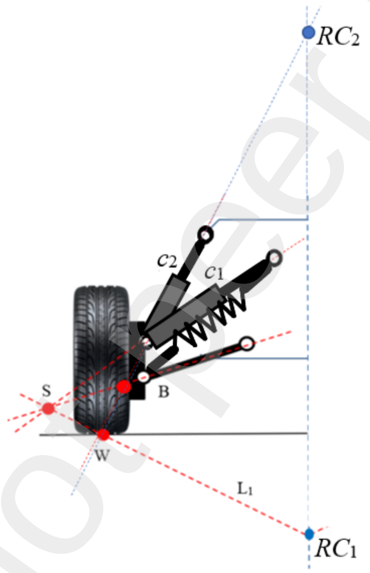

Fig. 16. Schematic of the *multi-damper* suspension for driving of the roll centre from RC_1 to RC_2.

The alternative solution proposed here is that of equipping the system with a suspension mechanism of the type shown in Fig. 16, defined as *multi-damper* suspension architecture. For each wheel, a double upper arm pivots each arm about two distinct points, by a pair of dampers that control the sliding couplers.

Fig. 16 emphasizes the driving of the roll centre: if $c_1 \rightarrow +\infty$ and $c_2 = 0$ the roll centre is RC_1; if $c_1 = 0$ and $c_2 \rightarrow +\infty$ then the roll centre migrates to RC_2. The fine tuning of the four upper arms enables the system to move the roll centre within an entire region (as it will be clear later), adapting its position to kinematic constraints that can be defined and tracked by using the technique described in the previous sections of this paper.

The migration of the roll centre position helps in the indirect control of the inertia characteristics of the body, and consequently of its instant natural roll frequency. Indeed, such a particular suspension mechanism can be used to reduce the roll angle of a vehicle when cornering, and simultaneously reduce vertical jerking in straight motion over a rough road.

To show the benefits coming from equipping a vehicle with *multi-damper* suspensions, a specific case will be analysed: a vehicle body excited at its centre of mass by a harmonic lateral force at its roll resonant frequency, a prototype case including maneuvers of lateral shaking of the car body induced by rough left-right steering sequences.

4.1. A half-car model

The vehicle body of the car is modelled as a half-car planar mechanism. The Lagrangian formulation is used to derive the car dynamics when the double-arm suspension system and the *multi-damper* architecture are employed. In particular, an analogous mathematical procedure and dimensioning to those described in [46,47] will be considered.

4.1.1. Dynamics of the vehicle equipped with double-arm suspensions

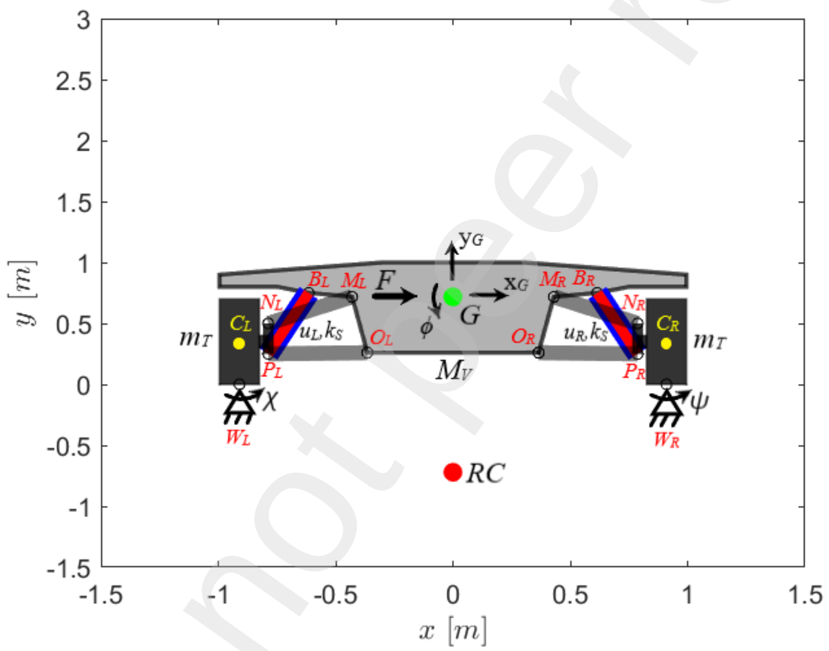

Fig. 17. Vehicle equipped with classic double-arm suspensions.

The vehicle equipped with the Double-Arm Suspension Systems (DASS) is represented in Fig. 17. It consists of a rigid body of mass M_V (with centre of mass G) which is linked to the two tire-wheel assemblies, each of mass m_T (with centres of mass C_L, C_R), through four rigid links (in transparent grey between points $M_L - N_L$, $M_R - N_R$, $O_L - P_L$, $O_R - P_R$) two telescopic linkages (in red between points $B_L - P_L$, $B_R - P_R$) characterized by controllable damping coefficients u_L,u_R and posed within two springs (in blue) with constant values k_S. In particular, the tire-wheel assemblies are considered as hinged to the frame in correspondence of the tires contact points W_L, W_R.

The vehicle system is characterized by the subsequent set of 5 Lagrangian variables $\boldsymbol{q} = [x_G \;\; y_G \;\; \phi \;\; \chi \;\; \psi]^T$, where the first 3 components describe, respectively, the planar displacements of the body car centre of mass G and the vehicle rotation about this point, while the last two components describe the lateral rotation of the tire-wheel assemblies with respect to the hinges (points W_L, W_R in Fig. 17).

Because of the presence of the four rigid links, the following four constraint equations must hold:

$$\begin{cases} \Gamma_1 = \left|\boldsymbol{x}_{M_L} - \boldsymbol{x}_{N_L}\right|^2 - l_{MN_L}^2 = 0 \\ \Gamma_2 = \left|\boldsymbol{x}_{M_R} - \boldsymbol{x}_{N_R}\right|^2 - l_{MN_R}^2 = 0 \\ \Gamma_3 = \left|\boldsymbol{x}_{O_L} - \boldsymbol{x}_{P_L}\right|^2 - l_{OP_L}^2 = 0 \\ \Gamma_4 = \left|\boldsymbol{x}_{O_R} - \boldsymbol{x}_{P_R}\right|^2 - l_{OP_R}^2 = 0 \end{cases} \tag{42}$$

where l_{MN_L},l_{MN_R},l_{OP_L},l_{OP_R} are the lengths of the four rigid links and the coordinates of the points of the vehicle and of the tire-wheel assemblies are:

$$\boldsymbol{x}_{M_L} = \boldsymbol{x}_G + \boldsymbol{R}_V \bar{\boldsymbol{x}}_{M_L} \tag{43}$$

$$\boldsymbol{x}_{M_R} = \boldsymbol{x}_G + \boldsymbol{R}_V \bar{\boldsymbol{x}}_{M_R} \tag{44}$$

$$\boldsymbol{x}_{O_L} = \boldsymbol{x}_G + \boldsymbol{R}_V \bar{\boldsymbol{x}}_{O_L} \tag{45}$$

$$\boldsymbol{x}_{O_R} = \boldsymbol{x}_G + \boldsymbol{R}_V \bar{\boldsymbol{x}}_{O_R} \tag{46}$$

$$\boldsymbol{x}_{N_L} = \boldsymbol{x}_{W_L} + \boldsymbol{R}_{T_L} \bar{\boldsymbol{x}}_{N_L} \tag{47}$$

$$\boldsymbol{x}_{N_R} = \boldsymbol{x}_{W_R} + \boldsymbol{R}_{T_R} \bar{\boldsymbol{x}}_{N_R} \tag{48}$$

$$\boldsymbol{x}_{P_L} = \boldsymbol{x}_{W_L} + \boldsymbol{R}_{T_L} \bar{\boldsymbol{x}}_{P_L} \tag{49}$$

with: $\boldsymbol{x}_G = [x_G \; y_G]^T$; $\bar{\boldsymbol{x}}_{M_L}$, $\bar{\boldsymbol{x}}_{M_R}$, $\bar{\boldsymbol{x}}_{O_L}$, $\bar{\boldsymbol{x}}_{O_R}$ the position vectors of the vehicle points in the vehicle mobile reference frame centred in G; $\bar{\boldsymbol{x}}_{N_L}$, $\bar{\boldsymbol{x}}_{N_R}$, $\bar{\boldsymbol{x}}_{P_L}$, $\bar{\boldsymbol{x}}_{P_R}$ the position vectors of the tires points in the tire-wheel assemblies mobile reference frames centred, respectively, in the two contact points W_L and W_R, of coordinates $\boldsymbol{x}_{W_L}$,$\boldsymbol{x}_{W_R}$ with respect to the fixed reference frame. $\boldsymbol{R}_V$ is the rotation matrix between the fixed and mobile body car frame and $\boldsymbol{R}_{T_L}$, $\boldsymbol{R}_{T_R}$ are the rotation matrices between the fixed and mobile frames of the left and right tires, *i.e.*:

$$\boldsymbol{R}_V = \begin{bmatrix} cos(\phi) & -sin(\phi) \\ sin(\phi) & cos(\phi) \end{bmatrix} \tag{50}$$

$$\boldsymbol{R}_{T_L} = \begin{bmatrix} cos(\chi) & -sin(\chi) \\ sin(\chi) & cos(\chi) \end{bmatrix} \tag{51}$$

$$\boldsymbol{R}_{T_R} = \begin{bmatrix} cos(\psi) & -sin(\psi) \\ sin(\psi) & cos(\psi) \end{bmatrix} \tag{52}$$

Therefore, the system shows a single d.o.f. This means its dynamics can be derived as function of a unique independent variable by expressing the others as functions of this one. However, since the constraint relationships in Eq. (42) are nonlinear, it would be difficult to obtain such dependence.

To simplify the problem, one could consider a linearization at the first order of the *j*-th constraint equation with respect to a generic time instant t_i, as:

$$\nabla_{\boldsymbol{q}}\Gamma_j|_{t_i} \cdot [\boldsymbol{q} - \boldsymbol{q}_{t_i}] + \Gamma_j|_{t_i} = 0 \quad j = 1,\ldots, 4 \tag{53}$$

where $\nabla_{\boldsymbol{q}}\Gamma_j$ is the gradient vector of Γ_j with respect to the Lagrangian variables vector $\boldsymbol{q}$.

Such linearized expressions represent a system of four algebraic equations in q_i. Thus, it is possible to obtain the expression of the dependent Lagrangian variables as functions of ϕ (which is chosen to be the independent variable), as:

$$x_G = \tilde{x}_G(\frac{\partial\Gamma_j}{\partial\boldsymbol{q}}|_{t_i}, \Gamma_j|_{t_i}, \phi) \tag{54}$$

$$y_G = \tilde{y}_G(\frac{\partial\Gamma_j}{\partial\boldsymbol{q}}|_{t_i}, \Gamma_j|_{t_i}, \phi) \tag{55}$$

$$\chi = \tilde{\chi}(\frac{\partial\Gamma_j}{\partial\boldsymbol{q}}|_{t_i}, \Gamma_j|_{t_i}, \phi) \tag{56}$$

$$\psi = \tilde{\psi}(\frac{\partial\Gamma_j}{\partial\boldsymbol{q}}|_{t_i}, \Gamma_j|_{t_i}, \phi) \tag{57}$$

The Lagrangian formulation is then considered to produce the equation of motion of the vehicle system, which can be written as:

$$\frac{d}{dt}\left(\frac{\partial K}{\partial \dot{q}_i}\right) - \frac{\partial K}{\partial q_i} + \frac{\partial D}{\partial \dot{q}_i} + \frac{\partial U}{\partial q_i} = \frac{\delta W}{\delta q_i} \qquad i = 1, \ldots, n \tag{58}$$

where, in this case, $n = 1$ since the system possesses 1 d.o.f.

Being K, D, U, respectively, the kinetic energy, the potential dissipative energy, the potential elastic energy of the system, and δW the virtual work done by the external forces, they are expressed as:

$$K = \frac{1}{2}M_V\left(\dot{x}_G^2 + \dot{y}_G^2\right) + \frac{1}{2}J_{V_G}\dot{\phi}^2 + \frac{1}{2}J_{T_{W_L}}\dot{\chi}^2 + \frac{1}{2}J_{T_{W_R}}\dot{\psi}^2 \tag{59}$$

$$D = \frac{1}{2}u_1 v_{PB_L}^2 + \frac{1}{2}u_2 v_{PB_R}^2 \tag{60}$$

$$U = \frac{1}{2}k_s \Delta l_{PB_L}^2 + \frac{1}{2}k_s \Delta l_{PB_R}^2 \tag{61}$$

$$\delta W = \left(\boldsymbol{F}_{c_V} + \boldsymbol{F}_{g_V}\right) \bullet \delta\boldsymbol{x}_G + \boldsymbol{F}_{g_{T_L}} \bullet \delta\boldsymbol{x}_{C_L} + \boldsymbol{F}_{g_{T_R}} \bullet \delta\boldsymbol{x}_{C_R} \tag{62}$$

with J_{V_G} be the moment of inertia of the vehicle body with respect to its centre of mass, $J_{T_{W_L}}$, $J_{T_{W_R}}$ be the moments of inertia of the two tire-wheel assemblies with respect to the corresponding contact points, that, by the Huygens-Steiner theorem, are:

$$J_{T_{W_L}} = J_{T_{C_L}} + m_T r_T^2 = J_{T_{W_R}} = J_{T_{C_R}} + m_T r_T^2 \tag{63}$$

and $J_{T_{C_L}}$, $J_{T_{C_R}}$ are the moments of inertia of the tire-wheel assemblies with respect to their centres of mass.

Moreover, it holds:

$$\Delta l_{PB_L} = l_{PB_{L_0}} - l_{PB_L} \tag{64}$$

$$\Delta l_{PB_R} = l_{PB_{R0}} - l_{PB_R} \tag{65}$$

$$l_{PB_L} = |\boldsymbol{x}_{B_L} - \boldsymbol{x}_{P_L}| \tag{66}$$

$$l_{PB_R} = |\boldsymbol{x}_{B_R} - \boldsymbol{x}_{P_R}| \tag{67}$$

$$v_{PB_L} = \dot{\Delta} l_{PB_L} \tag{68}$$

$$v_{PB_R} = \dot{\Delta} l_{PB_R} \tag{69}$$

$$\boldsymbol{x}_{B_L} = \boldsymbol{x}_G + \boldsymbol{R}_V \bar{\boldsymbol{x}}_{B_L} \tag{70}$$

$$\boldsymbol{x}_{B_R} = \boldsymbol{x}_G + \boldsymbol{R}_V \bar{\boldsymbol{x}}_{B_R} \tag{71}$$

$$\boldsymbol{x}_{P_L} = \boldsymbol{x}_{W_L} + \boldsymbol{R}_{T_L} \bar{\boldsymbol{x}}_{P_L} \tag{72}$$

$$\boldsymbol{x}_{P_R} = \boldsymbol{x}_{W_R} + \boldsymbol{R}_{T_R} \bar{\boldsymbol{x}}_{P_R} \tag{73}$$

In particular: $l_{PB_{L_0}}$,$l_{PB_{R_0}}$ describe the initial distances between points $P_L - B_L$, $P_R - B_R$; $\bar{\boldsymbol{x}}_{B_L}$, $\bar{\boldsymbol{x}}_{B_R}$, $\bar{\boldsymbol{x}}_{P_L}$, $\bar{\boldsymbol{x}}_{P_R}$ are the position vectors of the points in the mobile reference frames of the body vehicle and the tire-wheel assemblies; $\boldsymbol{F}_{c_V} = [F(t)\ 0]^T$, $\boldsymbol{F}_{g_V} = [0 - M_V g]^T$, $\boldsymbol{F}_{g_{T_L}} = \boldsymbol{F}_{g_{T_R}} = [0 - m_T g]^T$ are, respectively, the lateral harmonic force acting on the centre of mass of the body car and the gravity force vectors acting on G and on the centres of mass C_{t_L},C_{t_R} of the two tires. Furthermore, $\delta\boldsymbol{x}_G$, $\delta\boldsymbol{x}_{C_L}$, $\delta\boldsymbol{x}_{C_R}$ represent the virtual displacements of the corresponding points, that can be defined as:

$$\delta\boldsymbol{x}_G = [\delta x_G\ \delta y_G]^T \tag{74}$$

$$\delta\boldsymbol{x}_{C_L} = \tilde{\boldsymbol{\Omega}}_{T_L} \boldsymbol{R}_{T_L} \bar{\boldsymbol{x}}_{C_L} \tag{75}$$

$$\delta\boldsymbol{x}_{C_R} = \tilde{\boldsymbol{\Omega}}_{T_R} \boldsymbol{R}_{T_R} \bar{\boldsymbol{x}}_{C_R} \tag{76}$$

with:

$$\tilde{\boldsymbol{\Omega}}_{T_L} = \begin{bmatrix} 0 & -\delta\chi \\ \delta\chi & 0 \end{bmatrix} \tag{77}$$

$$\tilde{\boldsymbol{\Omega}}_{T_R} = \begin{bmatrix} 0 & -\delta\psi \\ \delta\psi & 0 \end{bmatrix} \tag{78}$$

Since the dependent variables x_G, y_G, χ, ψ can be expressed in terms of ϕ, their time derivatives can be computed simply by deriving with respect to time the relationships in Eq. (54)-(57): $\dot{x}_G = \frac{\partial \tilde{x}_G}{\partial \phi}\dot{\phi}$, $\dot{y}_G = \frac{\partial \tilde{y}_G}{\partial \phi}\dot{\phi}$, $\dot{\chi} = \frac{\partial \tilde{\chi}}{\partial \phi}\dot{\phi}$, $\dot{\psi} = \frac{\partial \tilde{\psi}}{\partial \phi}\dot{\phi}$. And the same kind of relationships can be produced between the virtual displacements of the dependent variables and $\delta\phi$, as: $\delta x_G = \frac{\partial \tilde{x}_G}{\partial \phi}\delta\phi$, $\delta y_G = \frac{\partial \tilde{y}_G}{\partial \phi}\delta\phi$, $\delta\chi = \frac{\partial \tilde{\chi}}{\partial \phi}\delta\phi$, $\delta\psi = \frac{\partial \tilde{\psi}}{\partial \phi}\delta\phi$.

Finally, one can substitute the previous expressions into Eq. (59)-(62) and then into Eq. (58) to obtain the dynamics of the vehicle equipped with the double-arm suspensions, which can be written as:

$$J_\phi \ddot{\phi} = Q_\phi - \frac{\partial D}{\partial \dot{\phi}} - \frac{\partial U}{\partial \phi} \tag{79}$$

where Q_ϕ is the Lagrangian component of the external forces associated with the independent variable ϕ, and J_ϕ is the resulting inertia term coming from $\frac{d}{dt}\left(\frac{\partial K}{\partial \dot{\phi}}\right)$.

The Eq. (79) can then be attacked by the iterative LQR scheme (see Appendix).

4.1.2. Dynamics of the vehicle equipped with multi-damper suspensions

To derive the vehicle dynamics in case the vehicle is equipped with the *Multi-Damper* Supension Systems (MDSS) one can follow the same procedure prieviously outlined with some modifications.

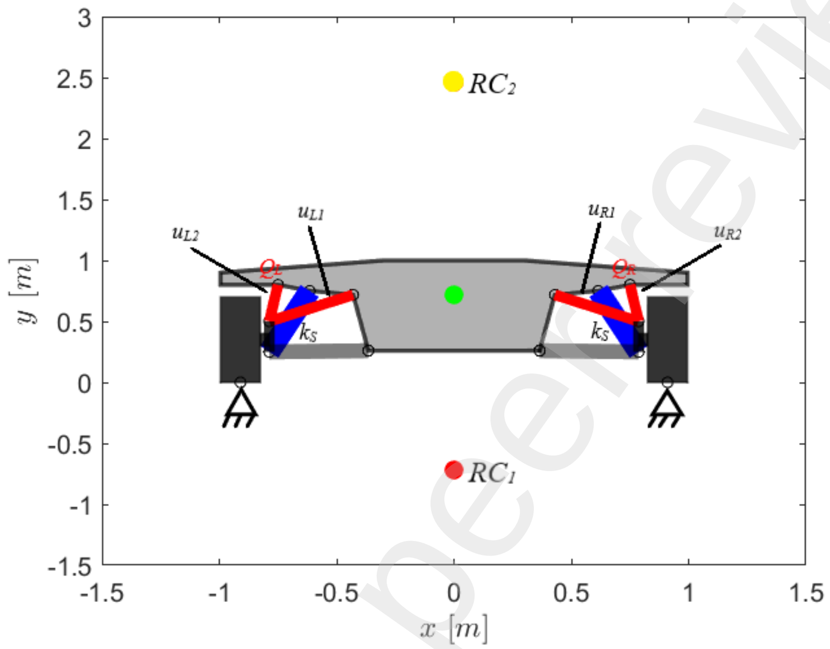

Fig. 18. Vehicle equipped with *multi-damper* suspensions.

In this situation, the system shows, in general, 3 d.o.f. By observing Fig. 18, the points of attachement of the suspensions to the vehicle are the same seen for the DASS, except for the definition of the new vehicle points Q_L, Q_R. They are necessary to introduce the two new Upper Tunable Dampers (UTDs) between points $Q_L - N_L$ and $Q_R - N_R$, of controllable damping coefficients u_{L_2}, u_{R_2}, respectively.

Now there are only two rigid links, and so only two of the original four constraint equations hold: Γ_3 and Γ_4 in Eq. (42). Indeed, the old upper rigid links (between points $M_L - N_L$ and $M_R - N_R$) have been replaced with two Lower Tunable Dampers (LTDss) of controllable damping coefficients u_{L_1}, u_{R_1}, respectively. The position of the springs is the same as for the DASS case, but they are not coupled with the dampers, as before.

The Lagrangian variables x_G,y_G,ϕ are chosen now as the independent variables, while χ,ψ remain the dependent ones, that can be expressed with analagous functions to those produced in Eq. (56), (57).

By defining with $\tilde{K}$,$\tilde{D}$,$\tilde{U}$,$\tilde{W}$ the kinetic, potential dissipative, potential elastic energies and the virtual work done by the external forces for this architecture, the system dynamics passes through the Lagrangian approach in Eq. (58), as before, with $n = 3$ and $\boldsymbol{q} = [x_G\ y_G\ \phi]^T$.

The main difference is in the definition of the new potential dissipative energy, which now is:

$$\tilde{D} = \frac{1}{2}u_{L_1}v_{MN_L}^2 + \frac{1}{2}u_{R_1}v_{MN_R}^2 + \frac{1}{2}u_{R_2}v_{QN_R}^2 + \frac{1}{2}u_{L_2}v_{QN_L}^2 \tag{80}$$

and, by following the same process seen for the DASS situation, the dynamics of the vehicle equipped with MDSS becomes:

$$\begin{cases} \tilde{m}_{x_G}\ddot{x}_G = \tilde{Q}_{x_G} - \frac{\partial \tilde{D}}{\partial \dot{x}_G} - \frac{\partial \tilde{U}}{\partial x_G} \\ \tilde{m}_{y_G}\ddot{y}_G = \tilde{Q}_{y_G} - \frac{\partial \tilde{D}}{\partial \dot{y}_G} - \frac{\partial \tilde{U}}{\partial y_G} \\ \tilde{J}_{\phi}\ddot{\phi} = \tilde{Q}_{\phi} - \frac{\partial \tilde{D}}{\partial \dot{\phi}} - \frac{\partial \tilde{U}}{\partial \phi} \end{cases} \tag{81}$$

where $\tilde{m}_{x_G}$, $\tilde{m}_{y_G}$,$\tilde{J}_{\phi}$ are resulting inertia terms coming from $\frac{d}{dt}\left(\frac{\partial \tilde{K}}{\partial \dot{x}_G}\right)$,$\frac{d}{dt}\left(\frac{\partial \tilde{K}}{\partial \dot{y}_G}\right)$,$\frac{d}{dt}\left(\frac{\partial \tilde{K}}{\partial \dot{\phi}}\right)$.

In reality, the number of d.o.f. of a vehicle system equipped with *multi-damper* suspensions depends on the particular setting of the UTDs and LTDs. In fact, for an arbitrary setting of both UTDs and LTDs, the system shows the 3 d.o.f., and so the dynamics is the one just described. But, in case of very large value of damping coefficients imposed for UTDs or LTDs ($c \simeq [10^7, 10^8]$ N s m^{-1}) the corresponding links behave as rigid connectors, causing the number of d.o.f. to collapse to only one. If this happens for the UTDs, the roll centre coincides with RC_2 (see Fig. 18) if this happens for the LTDs, the MDSS emulates the DASS and, in this case, its roll centre coincides with RC_1), which in fact represents the *kinematic roll centre* of the standard double-arm suspension system (compare Fig. 18 and Fig. 17).

Again, the system in Eq. (81) can be easily attacked by the iterative LQR scheme (see Appendix).

4.2. Control of the vehicle roll response in roll resonant conditions

Two cases are considered when using the MDSS: (i) the LTDs are settled to a constant very large damping value and the UTDs are indeed tunable, which means only the UTDs are controlled (this solution will be labelled as $MDSS_{2D}$); (ii) both the LTDs and the UTDs are tunable (this solution will be labelled as $MDSS_{4D}$). Both of these solutions are compared with the purely passive DASS arrangement in the absence of control, where the damping coefficients are set both to c_0 (this solution will be labelled as free) and the solution obtained by applying the control scheme even in the DASS case (this solution will be labelled as $DASS$).

For the DASS and MDSS cases, the state vectors are respectively defined as:

$$\boldsymbol{x}_{DASS} = [\phi \; \dot{\phi}]^T \tag{82}$$

$$\boldsymbol{x}_{MDSS} = [x_G \; y_G \; \phi \; \dot{x}_G \; \dot{y}_G \; \dot{\phi}]^T \tag{83}$$

Depending if the vehicle is equipped with the DASS or the MDSS, the objective function provided to the iterative LQR scheme has to be different too.

Since the controller has to reduce the roll oscillation of the vehicle, the target state vectors can be defined, respectively, as:

$$\boldsymbol{x}_{r_{DASS}} = [0 \; 0]^T \tag{84}$$

$$\boldsymbol{x}_{r_{MDSS}} = [x_G \; y_G \; 0 \; \dot{x}_G \; \dot{y}_G \; 0]^T \tag{85}$$

Nevertheless, in the MDSS case, one could improve the objective function by providing a further information to the controller, that is related to the error between the current RC position and its target position. Indeed, one could consider as target for this point the current position of the vehicle centre of mass, to try to reduce the available arm for the external excitation, and so to mitigate the roll angle and angular velocity. This additional condition is imposed in an indirect form, *i.e.* by transforming the target requirement on the position of RC as a target requirement on the velocity vector of G.

Therefore, if the target roll centre $RC_r = G$, it means the target velocity vector for the centre of mass must be:

$$\boldsymbol{v}_{G_r} = \boldsymbol{\Omega}(\boldsymbol{x}_G - \boldsymbol{x}_{RC_r}) = [0\ 0]^T \tag{86}$$

with:

$$\boldsymbol{\Omega} = \begin{bmatrix} 0 & -\dot{\phi} \\ \dot{\phi} & 0 \end{bmatrix} \tag{87}$$

and so, the expression of the target state vector for the MDSS (both $MDSS_{2D}$ and $MDSS_{4D}$) architecture can be updated to be:

$$\boldsymbol{x}_{r_{MDSS}} = [x_G\ y_G\ 0\ 0\ 0\ 0]^T \tag{88}$$

The controllable damping vector will assume the subsequent forms depending on the examined situation:

$$\boldsymbol{u}_{DASS} = \overline{\boldsymbol{R}}^{-1}\boldsymbol{B}^T[\boldsymbol{S}[\boldsymbol{x} - \boldsymbol{x}_{r_{DASS}}] + \boldsymbol{p}] - \boldsymbol{\Theta}(\boldsymbol{x}_{r_{DASS}})^+[\boldsymbol{\Phi}(\boldsymbol{x}_{r_{DASS}}) + \boldsymbol{d}] \tag{89}$$

$$\boldsymbol{u}_{MDSS} = \overline{\boldsymbol{R}}^{-1}\boldsymbol{B}^T[\boldsymbol{S}[\boldsymbol{x} - \boldsymbol{x}_{r_{MDSS}}] + \boldsymbol{p}] - \boldsymbol{\Theta}(\boldsymbol{x}_{r_{MDSS}})^+[\boldsymbol{\Phi}(\boldsymbol{x}_{r_{MDSS}}) + \boldsymbol{d} - \dot{\boldsymbol{x}}_{r_{MDSS}}] \tag{90}$$

with $[1, 50]$ kN s m^{1} as the admissable set for the damping coefficients values.

4.2.1. Simulation results

To perform the simulations the following dimensioning has been adopted [46,47]: $M_V = 878.76$ kg, $J_{V_G} = 247$ kg m^2, $m_T = 42.27$ kg, $r_T = 0.35$ m, $J_{T_{C_L}} = J_{T_{C_R}} = 1.86$ kg m^2, $k_S = 38404$ N m^{-1}. The starting position vector of the points of the vehicle and tire-wheel assemblies, given in the fixed reference frame, are: $\boldsymbol{x}_{G_0} = [0\ 0.718]^T$, $\boldsymbol{x}_{M_{L_0}} = [-0.43\ 0.718]^T$, $\boldsymbol{x}_{O_{L_0}} = [-0.365\ 0.26]^T$, $\boldsymbol{x}_{Q_{L_0}} = [-0.75\ 0.8]^T$, $\boldsymbol{x}_{N_{L_0}} = [-0.787\ 0.5]^T$, $\boldsymbol{x}_{P_{L_0}} = [-0.787\ 0.25]^T$, $\boldsymbol{x}_{C_{L_0}} = [-0.91\ 0.35]^T$, $\boldsymbol{x}_{W_{L_0}} = [-0.91\ 0]^T$, $\boldsymbol{x}_{M_{R_0}} = [0.43\ 0.718]^T$, $\boldsymbol{x}_{O_{R_0}} = [0.365\ 0.26]^T$, $\boldsymbol{x}_{Q_{R_0}} = [0.75\ 0.8]^T$, $\boldsymbol{x}_{N_{R_0}} = [0.787\ 0.5]^T$, $\boldsymbol{x}_{P_{R_0}} = [0.787\ 0.25]^T$, $\boldsymbol{x}_{C_{R_0}} = [0.91\ 0.35]^T$, $\boldsymbol{x}_{W_{R_0}} = [0.91\ 0]^T$.

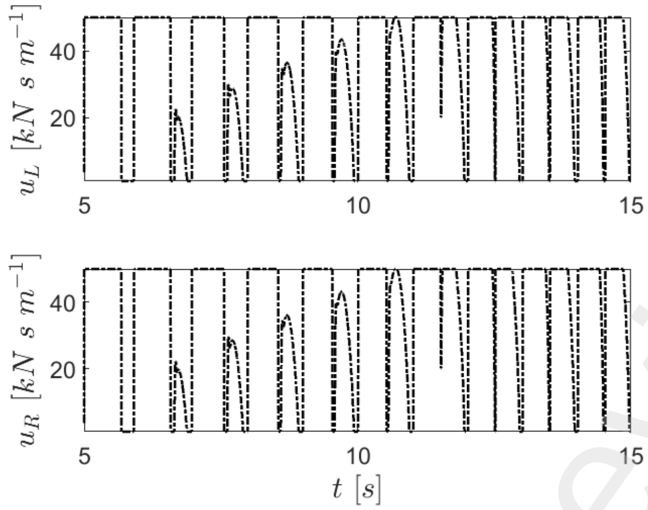

Fig. 19. Optimal damping coefficients for the controlled $DASS$ case.

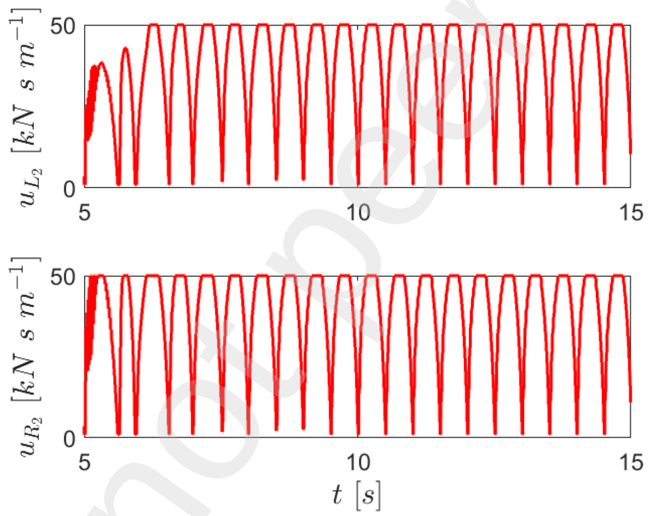

Fig. 20. Optimal damping coefficients for the controlled $MDSS_{2D}$ case.

The selected parameters, together with a starting value for the damping coefficients equal to $c_0 = 3593$ N s m^{-1}, produce, for the vehicle equipped with the DASS (or with the MDSS when the damping coefficients of the LTDs are set to very large values), a dampened roll resonant frequency $f_n^{roll} \simeq 1$ Hz, close to the standard one for real vehicles.

The observation time is $\overline{T} = 15$ s and, in this case, a timing for the controller action is imposed as $[5, 15]$ s to better appreciate the comparison between the uncontrolled and controlled responses for the different scenarios. Furthermore, the exciting lateral force is chosen as $F = 2sin(2\pi f_n^{roll} t)$ kN (see Fig. 17).

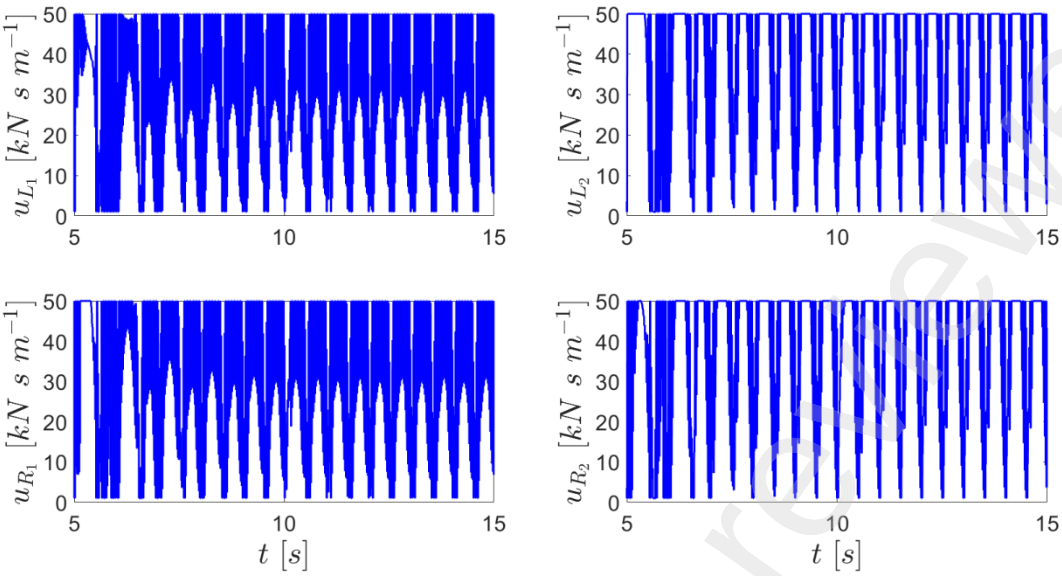

Fig. 21. Optimal damping coefficients for the controlled $MDSS_{4D}$ case.

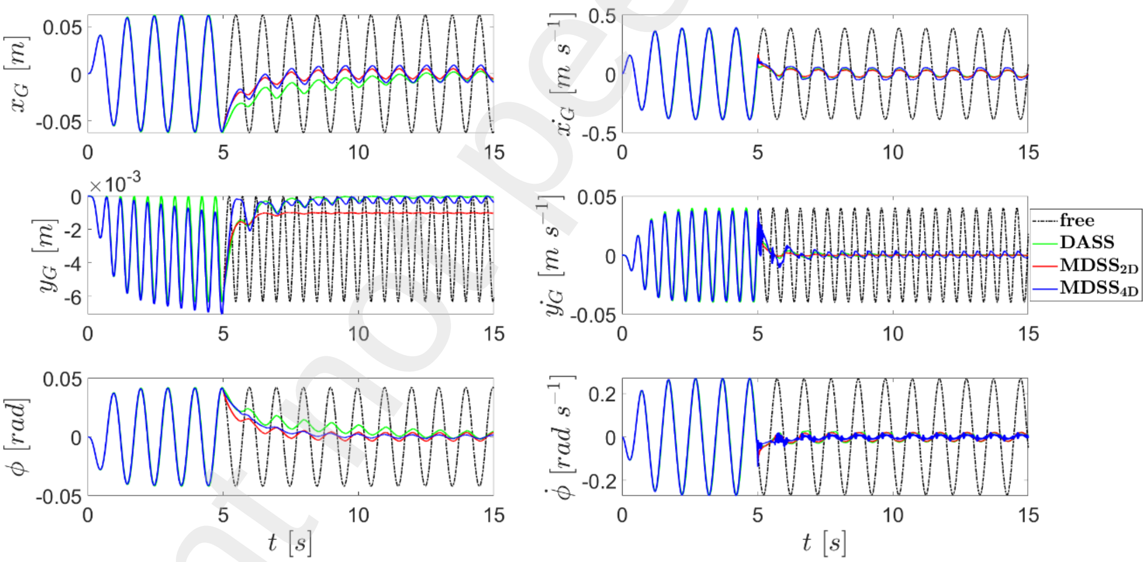

Fig. 22. Comparison between the free and controlled $DASS$, $MDSS_{2D}$,$MDSS_{4D}$ vehicle solutions.

Fig. 19, Fig. 20 and Fig. 21 represent the optimal damping values for the controlled $DASS$ solution and the $MDSS_{2D}$,$MDSS_{4D}$ schemes, respectively.

In short, all the control laws alternate between the two saturation extremes for the tunable dampers. It is also clear how the damping laws for the $MDSS_{4D}$ are characterized by a more complicated pattern with respect to those corresponding to the $DASS$ and $MDSS_{2D}$.

In Fig. 22 and Fig. 23, the comparison between the solutions for the vehicle and the tires, for all the four scenarios, is portrayed. While the free solution shows the expected resonant behavior, all the controlled solutions appear to dampen efficiently the system response.

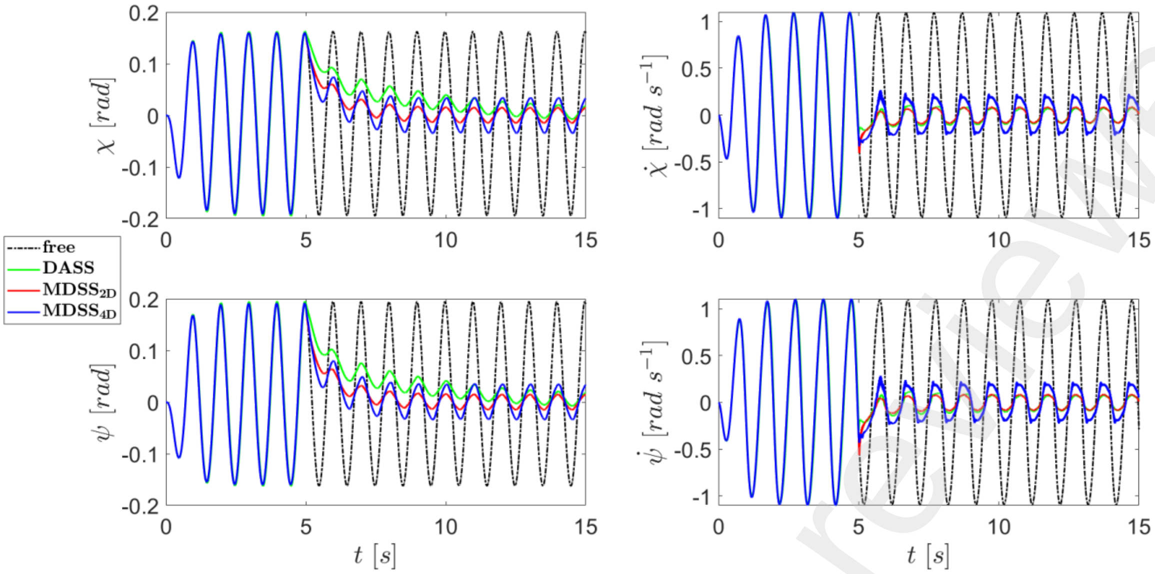

Fig. 23. Comparison between the free and controlled $DASS$, $MDSS_{2D}$,$MDSS_{4D}$ wheels solutions.

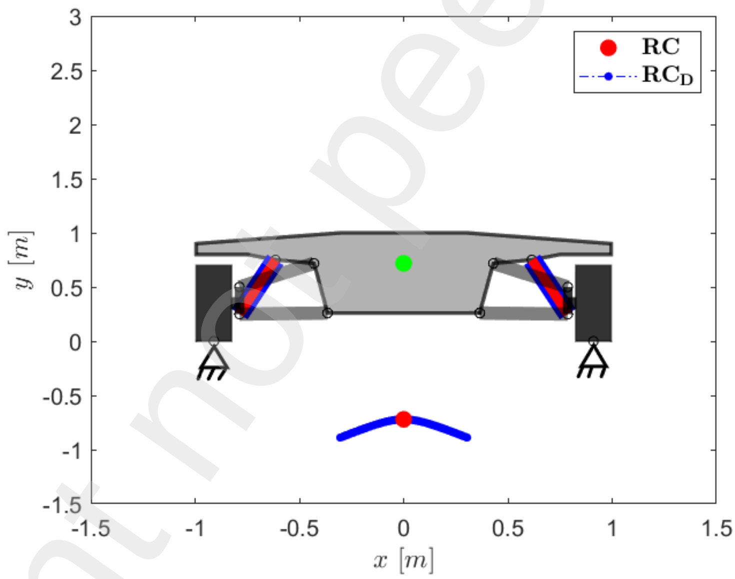

Fig. 24. Comparison between the *kinematic roll centre* RC and the *dynamic roll centre* RC_D for the free and controlled $DASS$ solutions.

Among them, the $MDSS_{2D}$ and $MDSS_{4D}$ stand out for the best results. If one focuses the attention on the roll angle and angular velocity quantities (see Fig. 22), the $MDSS_{4D}$ performs even better, confirming the benefits coming from the controllability of the overall $MDSS$ arrangement.

It is interesting to observe Fig. 24, Fig. 25 and Fig. 26.

Fig. 24 shows the behaviour of the *dynamic roll centre* RC_D for the free and controlled $DASS$ arrangements, computed through Eq. (1), compared with the *kinematic roll centre* position RC which coincides with the original roll centre position in Fig. 17. It appears how the RC_D is constrained to move along a curvilinear segment.

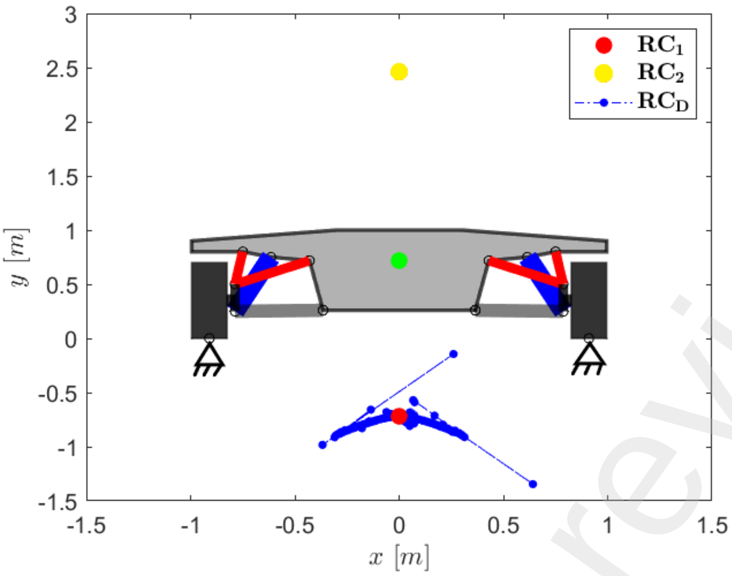

Fig. 25. Comparison between the *kinematic roll centres* RC_1, RC_2 and the *dynamic roll centre* RC_D for the $MDSS_{2D}$ controlled solution.

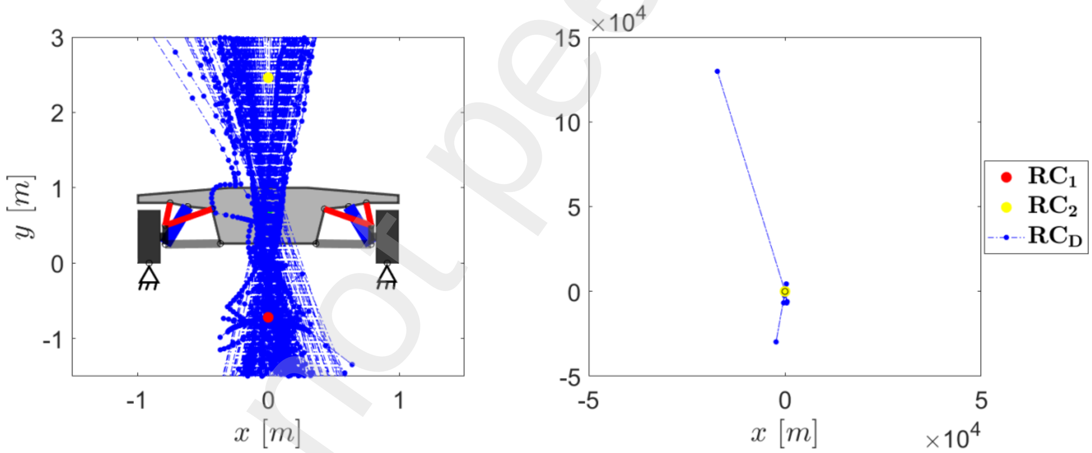

Fig. 26. Comparison between the *kinematic roll centres* RC_1, RC_2 and the *dynamic roll centre* RC_D for the $MDSS_{4D}$ controlled solution.

In the $MDSS_{2D}$ scheme (see Fig. 25), the *dynamic roll centre* RC_D spends most of the time close to the *kinematic roll centre* RC (defined by the DASS architecture), however it does not remain confined on the curvilinear path: in some instants, it moves away from it.

In the $MDSS_{4D}$ scheme (see Fig. 26), RC_D moves along a completely different and more complex pattern, produced by two new opposite conical branches with higher slope, and spending time even far from the two *kinematic roll centres* RC_1 and RC_2 (already observed in Fig. 18). In particular, left subplot of Fig. 26 shows a close up in the vicinity of the vehicle, of the roll center positions, , while on the right plot, the overall behavior is displayed. In this case RC_D reaches positions very far from the vehicle body.

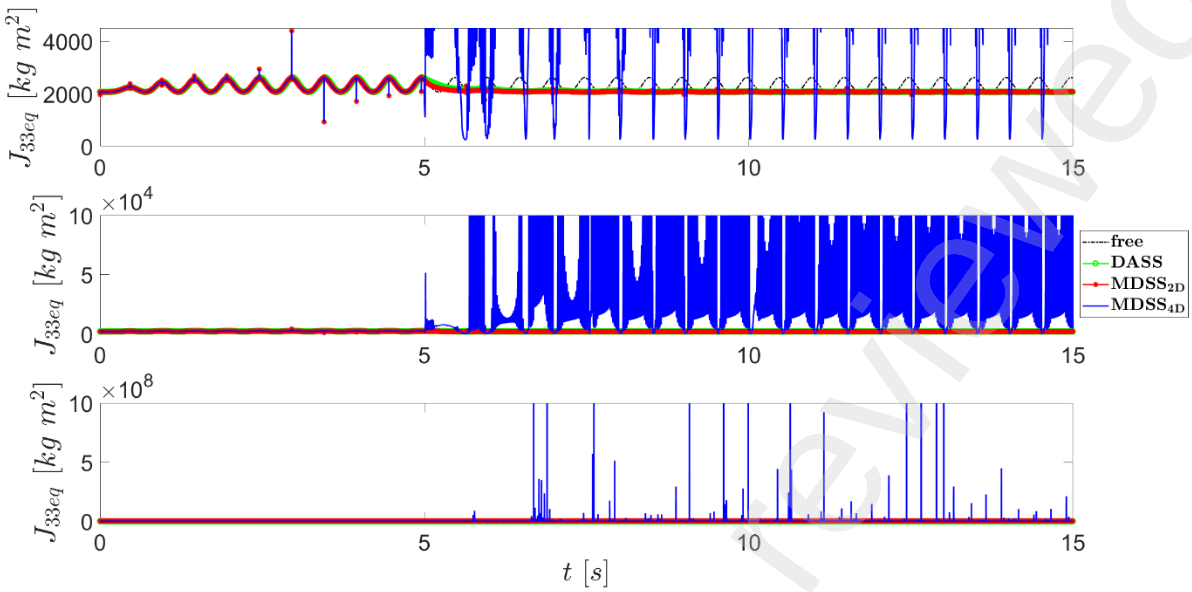

Fig. 27. Comparison between the *equivalent inertia tensor* element $J_{33_{eq}}$ for the free and controlled $DASS$, $MDSS_{2D}$,$MDSS_{4D}$ systems.

These effects are confirmed by examining the value of the roll (polar) moment of inertia of the vehicle, represented by the element $J_{33_{eq}}$ of the *equivalent inertia tensor* of the car body, and evaluated through Eq. (2). It is interesting to see how such quantity behaves differently from the roll moment of inertia obtained for the free solution, which is evaluated with respect to the *kinematic roll centre* of the $DASS$ arrangement RC, as shown in Fig. 17.

While the inertia value for the free solution maintains a harmonic behavior around the middle value of about 2300 kg m^2 (a little bit greater than the kinematic reference value of about 2000 kg m^2), even after the intervention of the controller (see Fig. 27), the $J_{33_{eq}}$ of the controlled $DASS$ and $MDSS_{2D}$ solutions is moved towards it. Thus, for these two cases, the control action has the effect of reducing the roll oscillation by reducing the roll moment of inertia.

On the other hand, the $J_{33_{eq}}$ of the $MDSS_{4D}$ solution shows very large values (see Fig. 27), that, of course, reflect the behavior of the corresponding RC_D, observed in Fig. 26. Therefore, for this arrangement, the control action causes an increase in the roll resistance of the body.

In all the cases, the roll moment of inertia follows specific periodic patterns (that reflect those coming from the damping control laws in Fig. 19, Fig. 20 and Fig. 21). If one inspects such patterns, they show a characteristic frequency of about 2 Hz, which is twice the roll resonant frequency of the original system and twice the exciting frequency.

This means the damping control move away the frequency response from the resonant conditions, originally at 1 Hz, with the effect of mitigating the roll amplitude. The response at frequencies other than those contained in the exciting force is a typical effect of nonlinear vibrational systems, and one of the most common is the doubling of the exciting frequency. In fact, it is clear the described damping control acts in a very nonlinear way, as emphasized by the analytical investigation of subsection 2.3, and the LQR linearization is valid only in a local approximation, where the system configuration does not change significantly with time.

Finally, because of the polodes control, the roll inertia is changing, and with it the roll instant frequency, in the context of a highly nonlinear process.

5. Conclusions

This paper investigates the possibility to control the kinematic characteristics of a body through the use of tunable dampers. The explored configurations include sliding couplers, each with a tunable damper, controlled by an Optimal Control Theory algorithm. The instant centre of rotation of the rigid body, *i.e.* its polode, is controlled by the damping of the sliders. As a remarkable effect, the inertia tensor of the body and instant natural frequencies change too.

The proposed theory shows the general form the problem takes by considering a generic 3D rigid body constrained through springs and telescopic linkages equipped with tunable dampers, where the control vector is the set of the tunable damping coefficients. Since the problem is highly nonlinear, Linear Quadratic Regulator is employed to determine the best instant tuning of the dampers.

A detailed application to the automotive suspension system is presented: the roll centre and axis of the car are semi-actively controlled by a set of four dampers, which provides a better mitigation of the system response in respect to a standard double-arm suspension architecture. The *multi-damper* suspension clearly shows the chance of reducing the roll angle of a vehicle body under roll resonant condition.

Acknowledgements

This work is supported by University of Rome, La Sapienza.

Appendix

The linearization procedure to derive the LQR control law is here defined.

The compact form of the system dynamics is represented by the following nonlinear differential equation, affine in the control term $\boldsymbol{u}$ as:

$$\dot{\boldsymbol{x}} = \boldsymbol{f}(\boldsymbol{x},\boldsymbol{u},\boldsymbol{y}) = \boldsymbol{\Phi}(\boldsymbol{x}) + \boldsymbol{\Theta}(\boldsymbol{x})\boldsymbol{u} + \boldsymbol{y} \tag{A.1}$$

The control statement consists in the minimization of the *functional* J^* with respect to the three *a priori* independent variables $\boldsymbol{x}, \boldsymbol{u}, \boldsymbol{\lambda}$ over an observation time $\overline{T}$, *i.e.*:

$$min\ (\boldsymbol{x}, \boldsymbol{u}, \boldsymbol{\lambda}) \quad J^* = \int_0^{\overline{T}} \{L(\boldsymbol{x},\boldsymbol{u},\boldsymbol{x}_r,\boldsymbol{u}_r) + \boldsymbol{\lambda}^T[\dot{\boldsymbol{x}} - \boldsymbol{f}(\boldsymbol{x},\boldsymbol{u},\boldsymbol{y})]\}\, dt \tag{A.2}$$

with $\boldsymbol{u} \in \overline{U}$ and by considering the initial condition on the system dynamics $\boldsymbol{x}(0) = \boldsymbol{x}_0$.

Since the linearization process passes through the LQR method, this means that the *penalty function* is $L(\boldsymbol{x},\boldsymbol{u},\boldsymbol{x}_r,\boldsymbol{u}_r) = \frac{1}{2}[\boldsymbol{x} - \boldsymbol{x}_r]^T\overline{\boldsymbol{Q}}[\boldsymbol{x} - \boldsymbol{x}_r] + \frac{1}{2}[\boldsymbol{u} - \boldsymbol{u}_r]^T\overline{\boldsymbol{R}}[\boldsymbol{u} - \boldsymbol{u}_r]$, with $\overline{\boldsymbol{Q}},\overline{\boldsymbol{R}}$ be the cost matrices on the errors on the state and control vectors, respectively. Thus, following the general approach [45], the iterative LQR control scheme in presence of target reference values imposed on both the state and control vectors, respectively defined with $\boldsymbol{x}_r, \boldsymbol{u}_r$, proceeds as follows.

The first requirement is that, once the system reached the target state, its dynamics must be $\dot{\boldsymbol{x}}_r$ (that in case of constant target is simply 0). Therefore, both $\boldsymbol{x}_r, \boldsymbol{u}_r$ must satisfy the following condition:

$$\dot{\boldsymbol{x}}_r = \boldsymbol{\Phi}(\boldsymbol{x}_r) + \boldsymbol{\Theta}(\boldsymbol{x}_r)\boldsymbol{u}_r + \boldsymbol{y} \tag{A.3}$$

and so, the control vector at the target state must be:

$$\boldsymbol{u}_r = -\,\boldsymbol{\Theta}(\boldsymbol{x}_r)^{+}[\boldsymbol{\Phi}(\boldsymbol{x}_r) + \boldsymbol{y} - \dot{\boldsymbol{x}}_r] \tag{A.4}$$

where the apex '+' represents the pseudo-inverse of the matrix $\boldsymbol{\Theta}(\boldsymbol{x}_r)$.

With the introduction of the target, the *functional* J^* can be rewritten as:

$$J^* = \int_0^{\overline{T}} \left\{\frac{1}{2}[\boldsymbol{x}-\boldsymbol{x}_r]^T\overline{\boldsymbol{Q}}[\boldsymbol{x}-\boldsymbol{x}_r] + \frac{1}{2}[\boldsymbol{u}-\boldsymbol{u}_r]^T\overline{\boldsymbol{R}}[\boldsymbol{u}-\boldsymbol{u}_r] + \boldsymbol{\lambda}^T[\dot{\boldsymbol{x}} - \boldsymbol{f}(\boldsymbol{x},\boldsymbol{u},\boldsymbol{y})]\right\}dt \tag{A.5}$$

To systematically apply the LQR algorithm, the second member in Eq. (A.1) is linearized with respect to variables $\boldsymbol{x},\boldsymbol{u}$ around the generic time instant t_i as follows:

$$\boldsymbol{\Phi}(\boldsymbol{x}) \simeq \boldsymbol{\Phi}(\boldsymbol{x}_{t_i}) + \nabla_{\boldsymbol{x}}\boldsymbol{\Phi}(\boldsymbol{x})|_{t_i}[\boldsymbol{x}-\boldsymbol{x}_{t_i}] \tag{A.6}$$

$$\begin{aligned}\boldsymbol{\Theta}(\boldsymbol{x})\boldsymbol{u} &\simeq \boldsymbol{\Theta}(\boldsymbol{x}_{t_i})\boldsymbol{u}_{t_i} + \nabla_{\boldsymbol{x}}[\boldsymbol{\Theta}(\boldsymbol{x})\boldsymbol{u}]|_{t_i}[\boldsymbol{x}-\boldsymbol{x}_{t_i}] + \nabla_{\boldsymbol{u}}[\boldsymbol{\Theta}(\boldsymbol{x})\boldsymbol{u}]|_{t_i}[\boldsymbol{u}-\boldsymbol{u}_{t_i}] = \\ &= \nabla_{\boldsymbol{x}}[\boldsymbol{\Theta}(\boldsymbol{x})\boldsymbol{u}]|_{t_i}[\boldsymbol{x}-\boldsymbol{x}_{t_i}] + \boldsymbol{\Theta}(\boldsymbol{x}_{t_i})\boldsymbol{u}\end{aligned} \tag{A.7}$$

where $\nabla_{\boldsymbol{b}}\boldsymbol{a}$ is the gradient of quantity $\boldsymbol{a}$ with respect to quantity $\boldsymbol{b}$. By substituting now the expressions in Eq. (A.6), (A.7) in Eq. (A.5) and by considering the subsequent change of coordinates $\tilde{\boldsymbol{x}} = \boldsymbol{x} - \boldsymbol{x}_r$, $\tilde{\boldsymbol{u}} = \boldsymbol{u} - \boldsymbol{u}_r$, the *i*-esimal *functional* J_i^* can be defined as:

$$J_i^* = \int_{t_i}^{t_i+\Delta t} \left\{\frac{1}{2}\tilde{\boldsymbol{x}}^T\overline{\boldsymbol{Q}}\tilde{\boldsymbol{x}} + \frac{1}{2}\tilde{\boldsymbol{u}}^T\overline{\boldsymbol{R}}\tilde{\boldsymbol{u}} + \boldsymbol{\lambda}^T\left[\dot{\boldsymbol{x}} - \left[\boldsymbol{\Phi}(\boldsymbol{x}_{t_i}) + \boldsymbol{A}[\tilde{\boldsymbol{x}} + \boldsymbol{x}_r - \boldsymbol{x}_{t_i}] + \boldsymbol{B}[\tilde{\boldsymbol{u}} + \boldsymbol{u}_r] + \boldsymbol{y}\right]\right]\right\}dt \tag{A.8}$$

with:

$$\boldsymbol{A} = \nabla_{\tilde{\boldsymbol{x}}+\boldsymbol{x}_r}\boldsymbol{\Phi}(\tilde{\boldsymbol{x}}+\boldsymbol{x}_r)|_{t_i} + \nabla_{\tilde{\boldsymbol{x}}+\boldsymbol{x}_r}[\boldsymbol{\Theta}(\tilde{\boldsymbol{x}}+\boldsymbol{x}_r)[\tilde{\boldsymbol{u}}+\boldsymbol{u}_r]]|_{t_i} \tag{A.9}$$

$$\boldsymbol{B} = \boldsymbol{\Theta}(\boldsymbol{x}_{t_i}) \tag{A.10}$$

By performing perturbations of J_i^* with respect to the three variables $\tilde{\boldsymbol{x}},\tilde{\boldsymbol{u}}, \boldsymbol{\lambda}$, it holds:

$$\begin{cases} \delta\tilde{\boldsymbol{x}}: \;\; \overline{\boldsymbol{Q}}\tilde{\boldsymbol{x}} - \boldsymbol{A}^T\boldsymbol{\lambda} - \dot{\boldsymbol{\lambda}} = \boldsymbol{0} \\ \delta\tilde{\boldsymbol{u}}: \;\; \overline{\boldsymbol{R}}\tilde{\boldsymbol{u}} - \boldsymbol{B}^T\boldsymbol{\lambda} = \boldsymbol{0} \\ \delta\boldsymbol{\lambda}: \;\; \dot{\tilde{\boldsymbol{x}}} - [\boldsymbol{\Phi}(\boldsymbol{x}_i) + \boldsymbol{A}[\tilde{\boldsymbol{x}} + \boldsymbol{x}_r - \boldsymbol{x}_i] + \boldsymbol{B}[\tilde{\boldsymbol{u}} + \boldsymbol{u}_r] + \boldsymbol{y}] = \boldsymbol{0} \end{cases} \tag{A.11}$$

By introducing the *Riccati Matrix* $\boldsymbol{S}$ and the *complementary term* $\boldsymbol{p}$, one could express $\boldsymbol{\lambda}$ as a function of the modified state $\tilde{\boldsymbol{x}}$ as:

$$\boldsymbol{\lambda}(\tilde{\boldsymbol{x}},t) = \boldsymbol{S}(t)\tilde{\boldsymbol{x}} + \boldsymbol{p}(t) \tag{A.12}$$

By substituting expression in Eq. (A.12) into the second equation in Eq. (A.11), it holds:

$$\tilde{\boldsymbol{u}}(\tilde{\boldsymbol{x}},t) = \overline{\boldsymbol{R}}^{-1}\boldsymbol{B}^T[\boldsymbol{S}(t)\tilde{\boldsymbol{x}} + \boldsymbol{p}(t)] \tag{A.13}$$

Now, by introducing the new expressions for $\boldsymbol{\lambda}, \tilde{\boldsymbol{u}}$ in Eq. (A.12), (A.13) into the first and third equations of Eq. (A.11), after some mathematics, the control problem assumes the form:

$$\begin{cases} \dot{\boldsymbol{S}} + \boldsymbol{A}^T\boldsymbol{S} + \boldsymbol{S}\boldsymbol{A} - \boldsymbol{S}\boldsymbol{B}\overline{\boldsymbol{R}}^{-1}\boldsymbol{B}^T\boldsymbol{S} + \overline{\boldsymbol{Q}} = \boldsymbol{0} \\ \dot{\boldsymbol{p}} + \boldsymbol{A}^T\boldsymbol{p} - \boldsymbol{S}\boldsymbol{B}\overline{\boldsymbol{R}}^{-1}\boldsymbol{B}^T\boldsymbol{p} - \boldsymbol{S}\overline{\boldsymbol{y}} = \boldsymbol{0} \end{cases} \tag{A.14}$$

with boundary conditions:

$$\begin{cases} \boldsymbol{S}(\overline{T}) = \boldsymbol{0} \\ \boldsymbol{p}(\overline{T}) = \boldsymbol{0} \end{cases} \tag{A.15}$$

and:

$$\overline{\boldsymbol{y}} = \boldsymbol{\Phi}(\boldsymbol{x}_{t_i}) + \boldsymbol{A}[\boldsymbol{x}_r - \boldsymbol{x}_{t_i}] + \boldsymbol{B}\boldsymbol{u}_r + \boldsymbol{y} \tag{A.16}$$

Therefore, the *i*-esimal optimal control feedback solution $\boldsymbol{u}$ in the original coordinates is:

$$\boldsymbol{u} = \tilde{\boldsymbol{u}} + \boldsymbol{u}_r = \overline{\boldsymbol{R}}^{-1}\boldsymbol{B}^T[\boldsymbol{S}(t)[\boldsymbol{x} - \boldsymbol{x}_r] + \boldsymbol{p}(t)] - \boldsymbol{\Theta}(\boldsymbol{x}_r)^+[\boldsymbol{\Phi}(\boldsymbol{x}_r) + \boldsymbol{y} - \dot{\boldsymbol{x}}_r] \tag{A.17}$$

References

[1] R. Isermann, Mechatronic Systems: Fundamentals, Springer, 2005.

[2] B. Fijakowski, Automotive Mechatronics: Operational and Practical Issues, Springer, 2011.

[3] A. Carcaterra, N. Roveri, Tire grip identification based on strain information: Theory and simulations, Mech. Syst. Signal Process. 41 (1)-(2) (2013) 564-580, https://doi.org/10.1016/j.ymssp.2013.06.002.

[4] N. Roveri, G. Pepe, A. Carcaterra, OPTYRE–A new technology for tire monitoring: Evidence of contact patch phenomena, Mech. Syst. Signal Process. 66-67 (2016) 793-810, https://doi.org/10.1016/j.ymssp.2015.06.019.

[5] F. Coppo, G. Pepe, N. Roveri, A. Carcaterra, A multisensing setup for the intelligent tire monitoring, Sensors 17 (3) (2017) 576, https://doi.org/10.3390/s17030576.

[6] M. J. Brennan, M. J. Day, R. J. Randall, An electrorheological fluid vibration damper, Smart Mater. Struct. 4 (1995) 83-92, 10.1088/0964-1726/4/2/003.

[7] S. B. Choi, Y. T. Choi, E. G. Chang, S. J. Han, C. S. Kim, Control characteristics of a continuously variable ER damper, Mechatron. 8 (2) (1998) 143-161, https://doi.org/10.1016/S0957-4158(97)00019-6.

[8] N. D. Sims, D. J. Peel, R. Stanway, A. R. Johnson, W. A. Bullough, The electrorheolgical long-stroke damper: A new modeling technique with experimental validation, J. Sound Vib. 229 (2) (2000) 207–227, https://doi.org/10.1006/jsvi.1999.2487.

[9] K. J. Kitching, D. J. Cole, D. Cebon, Performance of a semi-active damper for heavy vehicles, J. Dyn. Syst., Meas., Control 122 (3) (2000) 498–506, https://doi.org/10.1115/1.1286431.

[10] Y. Choi, N. M. Wereley, Assessment of Time Response Characteristics of Electrorheological and Magnetorheological Dampers, Proceedings of SPIE's 8th Annual International Symposium on Smart Structures and Materials 4331 (2001), Newport Beach, CA, United States, https://doi.org/10.1117/12.432693.

[11] Y. Choi, N. M. Wereley, Comparative Analysis of the Time Response of Electrorheological and Magnetorheological Dampers Using Nondimensional Parameters, J. Intell. Mater. Syst. Struct. 13 (7-8) (2002), https://doi.org/10.1106/104538902028557.

[12] PQ Xia, An inverse model of MR damper using optimal neural network and system identification, J. Sound Vib. 266 (5) (2003) 1009–1023, https://doi.org/10.1016/S0022-460X(02)01408-6.

[13] E. Guglielmino, K. A. Edge, A controlled friction damper for vehicle applications, Control Eng. Pract. 12 (4) (2004) 431–443, https://doi.org/10.1016/S0967-0661(03)00119-9.

[14] M. J. L. Boada, J. A. Calvo, B. L. Boada, V. Diaz, Modeling of a magnetorheological damper by recursive lazy learning, Int. J. Non-Linear Mech. 46 (3) (2011) 479-485, https://doi.org/10.1016/j.ijnonlinmec.2008.11.019.

[15] M. Bitaraf, O. E. Ozbulut, S. Hurlebaus, L. Barroso, Application of semi-active control strategies for seismic protection of buildings with MR dampers, Eng. Struct. 32 (2010) 3040-3047, https://doi.org/10.1016/j.engstruct.2010.05.023.

[16] O. Baser, H. Kizilhan, E. Kilic, Employing variable impedance (stiffness/damping) hybrid actuators on lower limb exoskeleton robots for stable and safe walking trajectory tracking, J. Mech. Sci. Technol. 34 (2020) 2597-2607, https://doi.org/10.1007/s12206-020-0534-4.

[17] M. Jiang, X. Rui, W. Zhu, F. Yang, J. Zhang, Modeling and control of magnetorheological 6-DOF stewart platform based on multibody systems transfer matrix method, Smart. Mater. Struct. 29 (3) (2020) 035029, https://doi.org/10.1088/1361-665X/ab675a.

[18] G. Pepe, I. Giorgio, A. Carcaterra, D. Del Vescovo, A. Sestieri, Semi-active vibration control via VFC-variational feedback by piezoelectric actuation, INTER-NOISE and NOISE-CON Congress and Conference/NOVEM2015/Proceedings 251 (1) (2015) 967-983, April 13-15, Dubrovnik, Croatia.

[19] E. Guglielmino, T. Sireteanu, C. W. Stammers, G. Ghita, M. Giuclea, Semi-active Suspension Control, Springer, 2008.

[20] S. M. Savaresi, C. Poussot-Vassal, C. Spelta, O. Sename, L. Dugard, Semi-Active Suspension Control Design for Vehicles, first ed., Elsevier, 2010.

[21] Z. B. lahcene, Dynamic and Control Analysis of Semi-Active Suspension System, LAMBERT Academic Publishing, 2010.

[22] S. Aubouet, Semi-Active Dampers Modeling and Control, LAMBERT Academic Publishing, 2010.

[23] C. Spelta, S. M. Savaresi, L. Fabbri, Experimental analysis of a motorcycle semi-active rear suspension, Control Eng. Pract. 18 (11) (2010) 1239-1250, https://doi.org/10.1016/j.conengprac.2010.02.006.

[24] C. Spelta, F. Previdi, S. M. Savaresi, P. Bolzern, M. Cutini, C. Bisaglia, Performance analysis with semi-active supensions with control of variable damping and stiffness, Veh. Syst. Dyn. Int. J. Veh. Mech. Mobil. 49 (1)-(2) (2011) 237-256, https://doi.org/10.1080/00423110903410526.

[25] C. Poussot-Vassal, C. Spelta, O. Sename, S. M. Savaresi, L. Dugard, Survey and performance evaluation on some automotive semi-active suspension control methods: A comparative study on a single-corner model, Annu. Rev. Control 36 (1) (2012) 148-160, https://doi.org/10.1016/j.arcontrol.2012.03.011.

[26] H. Metered, Z. Šika, Vibration control of a semi-active seat suspension system using magnetorheological damper, 2014 IEEE/ASME 10th International Conference on Mechatronic and Embedded Systems and Applications (MESA)/Proceedings 1-7 (2014), September 10-12, Senigallia, Italy, https://doi.org/10.1109/MESA.2014.6935527.

[27] G. Pepe, A. Carcaterra, A new semi-active variational based damping control, 2014 IEEE/ASME 10th International Conference on Mechatronic and Embedded Systems and Applications (MESA)/ Proceedings 1-7 (2014), September 10-12, Senigallia, Italy, https://doi.org/10.1109/MESA.2014.6935611.

[28] G. Pepe, A. Carcaterra, VFC-Variational Feedback Controller and its applications to semi-active suspensions, Mech. Syst. Signal Process. 76-77 (2016) 72-92, https://doi.org/10.1016/j.ymssp.2016.01.002.

[29] G. Pepe, A. Carcaterra, VFC-Variational Feedback Control applied to semi-active car suspensions, INTER-NOISE and NOISE-CON Congress and Conference/NOVEM2015/ Proceedings 251 (1) (2015) 952-966, April 13-15, Dubrovnik, Croatia.

[30] M. Q. Nguyen, M. Canale, O. Sename, L. Dugard, A Model Predictive Control approach for semi-active suspension control problem of a full car, Proceedings of 2016 IEEE 55th Conference on Decision and Control (CDC) (2016) 721-726, December 12-14, Las Vegas, USA, https://doi.org/10.1109/CDC.2016.7798353.

[31] P. W. Jensen, The polode synthesis method, Forsch Ing-Wes 58 (1992) 152–163, https://doi.org/10.1007/BF02574529.

[32] TT Fu, C.H Chiang, Simulating a given spherical motion by the polode method, Mech. Mach. Theory 29 (2) (1994) 237-249, https://doi.org/10.1016/0094-114X(94)90033-7.

[33] J. M. Jiménez, G. Álvarez, J. Cardenal, J. Cuadrado, A simple and general method for kinematic synthesis of spatial mechanisms, Mech. Mach. Theory 32 (3) (1997) 323-341, https://doi.org/10.1016/S0094-114X(96)00017-1.

[34] K. Russell, R. S. Sodhi, Instant screw axis point synthesis of the RRSS mechanism, Mech. Mach. Theory 37 (10) (2002) 1117-1126, https://doi.org/10.1016/S0094-114X(02)00047-2.

[35] G. Bai, D. Li, S. Wei, Q. Liao, Kinematics and synthesis of a type of mechanisms with multiple remote centers of motion, Proceedings of the Institution of Mechanical Engineers, Part C: J. Mech. Eng. Sci. 228 (18) (2014) 3430-3440, https://doi.org/10.1177/0954406214527915.

[36] S. Wang, D. Wang, W. Jia, New Approach for Rigid Body Guidance of Spherical Four-Bar Linkages, Proceedings of 2008 3rd International Conference on Innovative Computing Information and Control (2008) 412-412, June 18-20, Dalian, China, https://doi.org/10.1109/ICICIC.2008.383.

[37] M. Cera, M. Cirelli, E. Pennestrì, R. Salerno, P. P. Valentini, Path-Constrained Points synthesis of symmetric mechanisms for prescribed higher-order curvature features, Mech. Mach. Theory 167 (2022) 104562, https://doi.org/10.1016/j.mechmachtheory.2021.104562.

[38] N. P. Belfiore, A. Di Benedetto, E. Pennestrì, Fondamenti di meccanica applicata alle macchine, second ed., CEA – Casa Editrice Ambrosiana, 2011.

[39] A. E. Bryson, Applied Optimal Control: Optimization, Estimation and Control, first ed., Routledge, 1975.

[40] D. E. Kirk, Optimal Control Theory: An Introduction, Dover Publications Inc., 2004.

[41] G. Pepe, M. Laurenza, D. Antonelli, A. Carcaterra, A new optimal control of obstacle avoidance for safer autonomous driving, Proceedings of 2019 AEIT International Conference of Electrical and Electronic Technologies for Automotive (AEIT AUTOMOTIVE) (2019) 1-6, July 2-4, Turin, Italy, https://doi.org/10.23919/EETA.2019.8804549.

[42] D. Antonelli, L. Nesi, G. Pepe, A. Carcaterra, A novel control strategy for autonomous cars, Proceedings of 2019 American control Conference (ACC) (2019) 711-716, July 10-12, Philadelphia, USA, https://doi.org/10.23919/ACC.2019.8814944.

[43] G. Pepe, E. Paifelman, A. Carcaterra, Optimal feedback control law for viscoelastic materials with memory effects, EURODYN 2020/XI International Conference on Structural Dynamics/ Proceedings 1 (2020) 1445-1458 November 23-26, Athens, Greece, https://doi.org/10.47964/1120.9117.19567.

[44] E. Paifelman, G. Pepe, A. Carcaterra, An optimal indirect control of underwater vehicle, Int. J. Control 94 (2) (2021) 312-326, https://doi.org/10.1080/00207179.2019.1590737.

[45] B. D. O. Anderson, J. B. Moore, Optimal Control: Linear Quadratic Methods, Dover Publications Inc., 2007.

[46] K. P. Balike, S. Rakheja, I. Stiharu, Development of kineto-dynamic quarter-car model for synthesis of a double wishbone suspension, Veh. Syst. Dyn. 49 (1)-(2) (2011) 107-128, https://doi.org/10.1080/00423110903401905.

[47] K. P. Balike, S. Rakheja, I. Stiharu, Kineto-dynamic Performance Analysis of Vehicle with an Asymmetric Suspension Damper using a Roll-Plane Model, Int. J. Veh. Perform. 1 (1) (2013) 69-91, https://doi.org/10.1504/IJVP.2013.057786.